(NASA-CR-150689) FLUID MECHANICS OF CONTINUOUS FLOW ELECTROPHORESIS Final Report (Universities Space Research Association) 96 p HC A05/MF A01 CSCL 07D

N78-24303

Unclas
G3/25 20761

PRINCETON UNIVERSITY

Fluid Mechanics of Continuous Flow Electrophoresis

Final Report

Contract NAS-8-31349 Code 361

Prepared for
George C. Marshall Space Flight Center
Marshall Space Flight Center, Alabama 35812

Submitted by

Universities Space Research Association
P.O. Box 1892
Houston, Texas

D.A. Saville
D.A. Saville
Principal Investigator
Princeton University

S. Ostrach (DAS)
S. Ostrach
Co-Investigator
Case-Western Reserve
University

April 1978

TABLE OF CONTENTS

ABSTRACT

The following aspects of continuous flow electrophoresis were studied: flow and temperature fields, hydrodynamic stability, separation efficiency, and characteristics of wide-gap chambers (the SPAR apparatus). Simplified mathematical models were developed so as to furnish a basis for understanding the phenomena and comparison of different chambers and operating conditions. Studies of the hydrodynamic stability disclosed that a "wide-gap" chamber may be particularly sensitive to axial temperature variations which could be due to uneven heating or cooling. The mathematical model of the separation process includes effects due to the axial velocity, electro-osmotic cross-flow and electrophoretic migration, all including the effects of temperature dependent properties.

INTRODUCTION

Hydrodynamics plays varied roles in the continuous flow electrophoresis of small particles, in some situations the suspending fluid does little more than carry particles through the apparatus, in others the flow is so convoluted that electrophoretic separation is impossible. One of the complicating factors is the role of buoyancy forces which can destabilize the flow or establish an unfavorable, but steady laminar flow. To circumvent such problems it has been suggested that the apparatus be operated in a microgravity environment where, due to the reduced size of buoyancy forces, the chamber could be made larger and field strength increased. Then populations of large biological particles could be fractionated into narrow subpopulations on the basis of unique surface characteristics which are reflected in the electrophoretic mobility. Such an undertaking obviously requires careful evaluations of many types. The purpose of this investigation is to furnish a basis for understanding the hydrodynamic characteristics of the chamber and their effects on the separation process. Particular emphasis is placed on the role buoyancy plays in establishing the basic flow and affecting its stability.

Work began on this project in February of 1977 with the objective of assembling and evaluating current knowledge of the hydrodynamics of continuous flow electrophoresis. Four tasks were specified for the one year contract period:

(1) Develop models to describe the flow and temperature fields;

(2) Investigate the hydrodynamic stability of the flow field;

(3) Develop a model to predict electrophoretic separation efficiency;

(4) Review the SPAR apparatus and experiment.

Work on these tasks is complete insofar as it is covered by this contract and results are described in this report. The studies begun here continue under a separate NASA contract with Princeton University. The main part of the report is divided into two parts: SUMMARIES AND CONCLUSIONS, and DESCRIPTION OF RESULTS, where more detailed information is set forth.

SUMMARIES AND CONCLUSIONS

More detailed information on the various subjects is contained in the DESCRIPTION OF RESULTS sections, here we simply summarize and discuss conclusions.

Flow and Temperature Fields

The temperature field enters the problem because it alters the electrophoretic mobility of the particles and causes density contrasts which lead to buoyancy driven flows. The non-uniform temperature field itself derives from heat effects associated with the electric field and current. Although the field is three-dimensional, it is possible to simplify matters using perturbation methods. For present purposes we sought to establish the edge effects due to cooling through the side walls containing the electrodes (cf. Figure 1)*, the effects of temperature dependent conductivities for heat and electricity, and estimate time scales for thermal equilibration of the chamber.

The edge effects were found to be substantial in that they extend into the chamber for distances of 1-2 chamber thicknesses from each side. This alters the mobility of particles in these regions and has a dramatic effect on the flow through buoyancy effects. It was also found that the effects of temperature dependent conductivities were substantial, the calculated temperature rise being 70% larger for a wide-gap chamber (0.5 cm thick)* than that calculated assuming constant properties. Although temperature relaxation times for the fluid are only 10-15 seconds for a narrow-gap chamber (0.15 cm) 2-3 minutes are required to establish the steady field in a wide-gap chamber.

---

* Representative dimensions, fluid properties, operating conditions, etc., are summarized on Table I, p. 72. A schematic diagram is on p. 7.

FIGURE 1.

Schematic representation of an electrophoresis chamber.

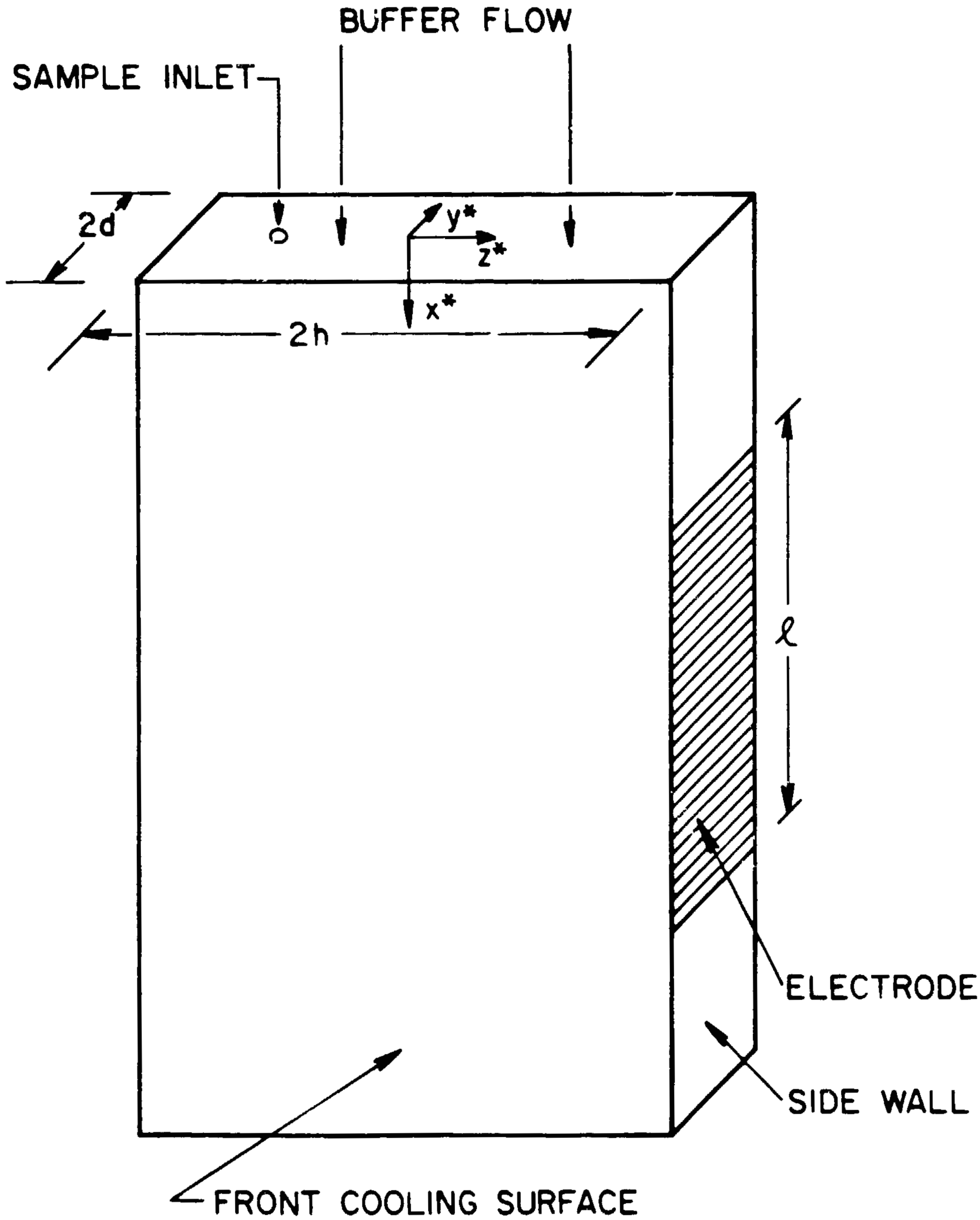

ORIGINAL PAGE IS
OF POOR QUALITY

For the flow field analytical solutions in two-dimensions were constructed to investigate ways buoyancy could alter the axial flow and to study edge effects. One-dimensional models were then developed to investigate the effects of temperature dependent transport properties on the axial flow and electro-osmotic cross flow.

Several conclusions can be drawn from this part of the study.

(a) It is necessary to include effects of temperature on transport properties. Models which ignore this, or treat matters inconsistantly, can be qualitatively and quantitatively misleading, especially with wide-gap machines like the SPAR device. With narrow-gap machines operated with modest field strengths (cf. Table 1) the use of 'average' values is satisfactory since temperature variations are usually small.

(b) In wide-gap machines operating in a 1-g environment the steady-state axial velocity profile is unsatisfactory at modest field strengths insofar as electrophoretic separations are concerned. An earlier study by Ostrach (using a 'constant properties' one-dimensional model) identified a buoyancy-driven feature which made downflow operation unsatisfactory. Edge effects and alterations due to temperature depending properties accentuate the buoyancy feature making matters worse. Upflow, which was once suggested as a means of overcoming the difficulty, turns out to be only marginally better for the cases studied. In downflow the difficulty arises from a recirculating eddy in the center of the chamber; in upflow two eddys appear, attached to the front and rear cooling surfaces, and these restrict the area available for separation. A micro-gravity environment would suppress or eliminate secondary flows of this sort. Of course other means of eddy suppression ought not be ruled out.

(c) Experiments at General Electric using the wide-gap SPAR apparatus disclosed a meandering sample flow pattern thought to be evidence of the structure noted in (b). Subsequent calculations made with the models developed here showed that the actual power levels were far lower than those required according to the theory and thus the meandering flow must be due to another process.

Hydrodynamic Stability

In an attempt to ascertain the cause of the meandering observed in the General Electric experiments the stability of several chamber configurations was examined. Attention focussed on buoyancy driven instabilities for obvious reasons and investigations of other sorts of instability, e.g., those due to viscosity stratification or electrokinetic effects, etc., were deferred. Three sorts of instability were investigated: the inception of cellular motion due to heat generation in a quiescent layer, roll cells in a buoyancy driven shear flow and the effect of an axial temperature gradient on a fully developed flow. Critical temperature differences for the quiescent layer or the shear flow are much larger than those present in the experiments. For the vertical chamber with axial flow a new two-dimensional instability was identified with an expecially low critical Rayleigh number. For conditions characteristic of the SPAR machine the critical axial gradient is (ca.) 0.5°C/cm.

Further experimental work will be required to establish whether or not the flow 'meandering' is a manifestation of the instability predicted by the current theory. If it is, then a micro-gravity environment will provide a means of avoiding it. Other types of instability mechanisms should also be investigated, however, so as to provide a comprehensive picture.

Prediction of Electrophoretic Separator Performance

Using the flow and temperature fields described earlier, a mathematical model of continuous electrophoretic separation was developed. The model (in brief):

(a) Accepts as input data the dimensions of the chamber, operating conditions and flowrates, transport properties of the buffer, location and size of the sample injection tube, mobility distribution of the sample, zeta-potential of the wall coating, number and size of the sample outlet streams, etc.

(b) Predicts the mobility distribution in each of the sample withdrawal streams.

Calculations were carried out using computer programs which have been tested on "model systems". Further refinements will be made under the current NASA contract with Princeton.

SPAR Electrophoresis Experiment

Throughout the course of this investigation attention focussed on understanding the behavior of wide-gap machines and predicting their performance. We now have models of the flow and temperature fields and can estimate the electrophoretic separation characteristics of a given device.

Although refinements will be necessary, the requisite 'first generation' models now exist for interpreting results from SPAR (or other) experiments. Furthermore, the effects of changes in process variables can be examined so as to optimize the separation.

Final Comments

Work begun during this program is being carried on under a joint program coordinated by Dr. R.S. Snyder of MSFC. These tasks include:

(a) Experimental studies (at MSFC) to ascertain the reason for flow meandering in wide-gap machines at 1-g. This will serve to prove or disprove the proposal that observed unsatisfactory operation is due to a buoyancy driven instability and assist in developing ways to circumvent the problem.

(b) Case-studies with the flow and separation models developed here to ascertain the ultimate (theoretical) capabilities of continuous flow devices.

(c) Theoretical work to extend the capabilities of the model, to develop an understanding of three-dimensional effects and finite sample concentration, and to investigate other hydrodynamic instabilities which could limit resolution. Establishing the limitations due to gravity and those arising from other phenomena.

Frequent observations of particle agglomeration and 'clumping' phenomena with cells underscore the need for an investigation of effects due to particle concentration. Recent theoretical studies (Batchelor, 1972) suggest substantial changes in sedimentation velocity at particle concentrations of a few percent but none of the extant studies deal with electrokinetic effects present in electrophoresis.

(d) The development of experimental techniques to test the model using mixtures of well-characterized particles. This will include micro-gravity experiments where appropriate

DESCRIPTION OF RESULTS

I. Flow and Temperature Fields

Introduction

Inside a continuous flow electrophoresis chamber of the sort depicted on Figure 1 the temperature and velocity have a three-dimensional character. Cold buffer enters one end of the chamber and adjusts to the new geometry within a distance, x_e, which is given roughly by the formula (Schlichting, 1960)

$$x_e = 0.16 \text{ Re } d. \tag{1}$$

Here d stands for the half-thickness and Re for the Reynolds nummer, $u_o d/\nu_o$; u_o is the mean axial velocity and ν_o the kinematic viscosity. Since the Reynolds number lies in the range 1-5, the entrance length is relatively short and here the velocity field can be modelled as being fully developed (viz. independent of x). As the buffer flow moves into the electrode region heat is added (volumetrically) through the action of the electric field and the associated current, so, to limit the temperature rise, the front and back walls are kept cold. For reasons that will be explained later (in the section on stability) the adjustment length for the temperature field can be substantial. Thus, in the electrode region the three-dimensional nature of the temperature field alters the structure of the velocity field through its effects on density and viscosity. Another contributory factor is the electro-osmotic cross-flow caused by the action of the field on the thin layer of charge in the fluid adjacent to the lateral boundaries. Although this velocity is typically much smaller than the axial velocity, it has a major role in altering the electrophoretic separation processes.

The models developed here to describe the temperature and velocity fields take advantage of three facts:

(i) The magnitude of the electro-osmotic velocity, w_o, is small compared to u_o.

(ii) The axial variation of the temperature is slow.

(iii) The effect of temperature on thermal conductivity and electrical conductivity is approximately linear over the temperature range of interest: 0° - 35°C.

These facts justify the use of perturbation methods to develop a description of the temperature and velocity fields. First, because of (i), the velocity field can be split into two parts, an axial flow field due to forced and natural convection with a superimposed electro-osmotic flow. Next, due to the slow variation of the transport properties with axial position, (ii), the velocity fields can be split into a fully-developed part (independent of x) with corrections added later to allow for axial structure. Finally, the simple linear variation, (iii), makes the description of the temperature field particularly simple.

Separate parts of the sequel are devoted to:

A. Mathematical models for the structure of the temperature field

   a. A two-dimensional model in which the effects of temperature on thermal conductivity are suppressed. This provides a means of evaluating edge-effects due to heat transfer near the side wall electrodes.

   b. A one-dimensional model to evaluate effects of a temperature dependent thermal conductivity.

   c. A transient heat conduction model to estimate thermal relaxation times.

B. Models for the structure of the axial velocity field

a. A two-dimensional, constant properties model provides a means of examining edge effects and buoyancy effects using the Boussinesq approximation.

b. A one-dimensional, variable properties model is the basis for evaluating thermal effects and is used in the separation model described in Part III.

C. Models for the electro-osmotic cross-flow velocity

a. A one-dimensional, variable properties model provides a basis for evaluating thermal effects and is used in the separation model (Part III).

Temperature Field

The equation for the conservation of thermal energy is

$$C_p \, u \frac{\partial T}{\partial x^*} = \nabla \cdot k \nabla T + \sigma_o E_o^2 \tag{2}$$

The symbols are: C_p - volumetric heat capacity, k - thermal conductivity, σ - electrical conductivity, and E_o - the electric field strength. E_o is assumed to be a constant throughout the analysis. Both k and σ vary with temperature in a linear fashion (see Figure 2) and so we write

$$\sigma = \sigma_o(1 + \sigma_1 \Theta) \tag{3}$$

$$k = k_o(1 + k_1 \Theta) \tag{4}$$

where k_o and σ_o are reference values evaluated at the wall temperature and Θ stands for a dimensionless temperature, i.e.,

FIGURE 2.

Thermal conductivity and electrical conductivity of the A-1 buffer.

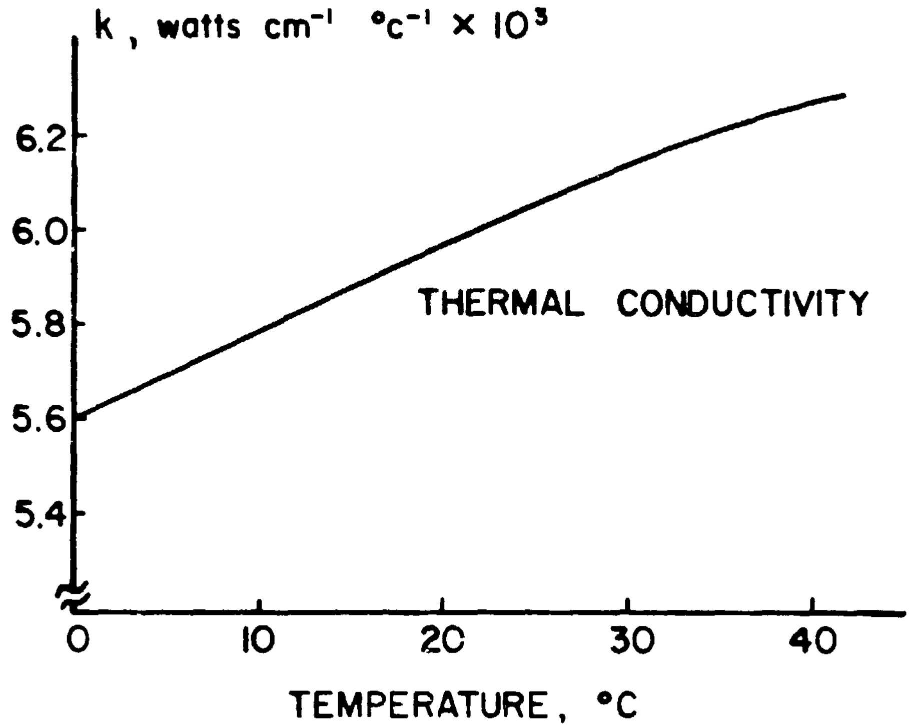
k, watts cm⁻¹ °c⁻¹ × 10³
6.2
6.0
5.8
5.6
5.4
THERMAL CONDUCTIVITY
0
10
20
30
40
TEMPERATURE, °C

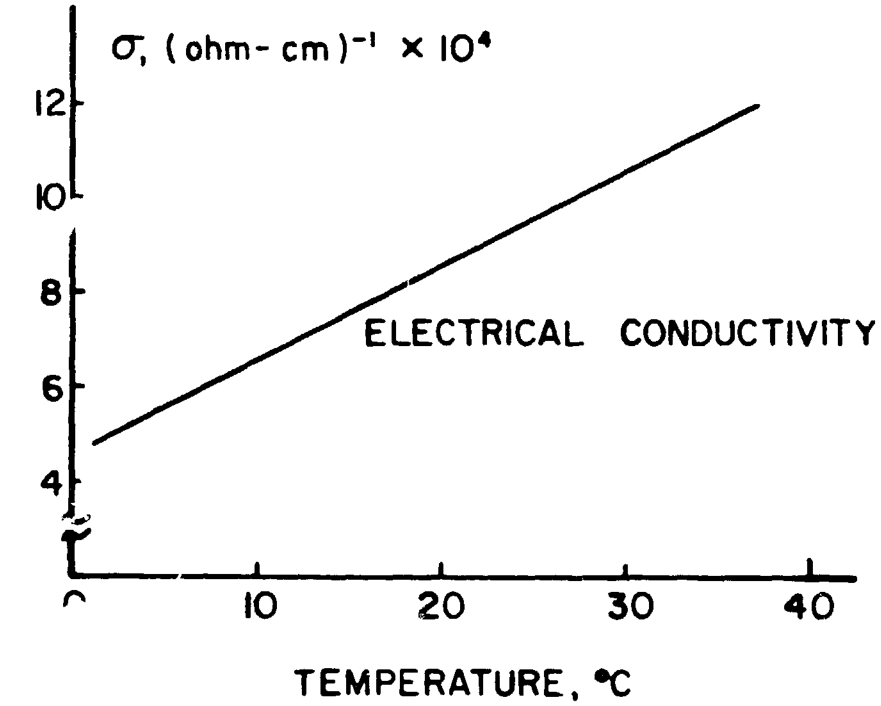
σ, (ohm-cm)⁻¹ × 10⁴
12
10
8
6
4
ELECTRICAL CONDUCTIVITY
10
20
30
40
TEMPERATURE, °C

2

$$T = T_w + \Delta T\ \Theta \tag{5}$$

The wall temperature is T_w and ΔT is a characteristic temperature difference. If we transform to dimensionless variables with u_o as the characteristic velocity and d the characteristic length, then

$$Pe\ u \frac{\partial\Theta}{\partial x} = \nabla\cdot[(1 + k_1\Theta)\nabla\Theta] + 1 + \sigma_1\Theta \tag{6}$$

where $Pe = C_p u_o d/k_o$ and $\Delta T = \sigma_o E_o^2 d^2/k_o$.

Both k_1 and σ_1 are less than unity: k_1 is typically $0(10^{-2})$ while σ_1 is $0(10^{-1})$, and so it is convenient to represent the temperature by means of a perturbation series in k_1, viz.

$$\Theta = \Theta^{(o)} + k_1\Theta^{(1)} + k_1^2\Theta^{(2)} + \ldots \tag{7}$$

Substituting into (6) we generate a sequence of equations for $\Theta^{(o)}$, $\Theta^{(1)}$, ...

$$Pe\ u \frac{\partial\Theta^{(o)}}{\partial x} = \nabla^2\Theta^{(o)} + \sigma_1\Theta^{(o)} + 1 \tag{8}$$

$$Pe\ u \frac{\partial\Theta^{(1)}}{\partial x} = \nabla^2\Theta^{(1)} + \sigma_1\Theta^{(1)} + \nabla\cdot(\Theta^{(o)}\nabla\Theta^{(o)}) \tag{9}$$

etc.

From equation (8) we deduce that in the thermal entrance region $\partial\Theta^{(o)}/\partial x$ is $0(Pe^{-1})$ and varies exponentially. Viscosity and density also depend on temperature so that a description of the temperature field to the order implied by equations (8) and (9) would entail an expansion for the axial velocity of the form

$$u = u^{(o)} + u^{(1)} + \ldots \tag{10}$$

ORIGINAL PAGE IS OF POOR QUALITY

where $u^{(o)}$ is the constant properties solution, $u^{(1)}$ accounts for temperature variations, etc. This expansion would be used to furnish complete velocity fields for (8) and (9). Because of the complexity of the problem it has not been practical here to attempt a solution which includes axial variations. Instead we have suppressed the axial structure and developed a 'zero-order' approximation with which we can assess the orders-of-magnitude of the thermal effects. An investigation of the details of the axial structure of the temperature and velocity fields is part of the work being done now under another NASA contract.

Two-Dimensional, Constant Thermal Conductivity Model

The major features of the fully developed temperature field can be found by solving equations (8) and (9), omitting the convective terms. The boundary conditions are:

(i) isothermal side walls, $\Theta = 0$, at $y = \pm 1$.

(ii) heat transfer through the side walls at $z = \pm H$ modelled in terms of a heat transfer coefficient, h, i.e.,

$$- k \frac{\partial T}{\partial z_*} = h_o(T - T_B).$$

T_B stands for the coolant temperature. For the zero-order field we have, in dimensionless form:

$$0 = - \nabla^2 \Theta^{(o)} + \sigma_1 \Theta^{(o)} + 1$$

$$\Theta^{(o)} = 0, \; y = \pm 1, \; \frac{\partial \Theta^{(o)}}{\partial z} = -Bi\, \Theta^{(o)}, \; z = \pm H \qquad (11)$$

The Biot number, Bi, is $h_o d/k_o$; $H = h/d$. For Bi = 0 the end walls are perfectly insulating and the temperature field is one-dimensional. For $Bi \to \infty$ the end walls are isothermal with $\Theta^{(o)} = 0$. Fourier transforms were used to solve equation (11) and the solution is

$$\Theta^{(o)}(y,z) = \frac{2}{\pi} \sum_{1}^{\infty} [A_n \cosh \lambda_n z + B_n] \sin \frac{n\pi}{2} (1 + y) \qquad (12)$$

where

$$A_n = \frac{Bi}{\lambda_n^2} \frac{(1+(-1)^n}{n} (\lambda_n \sinh \lambda_n H - Bi \cosh \lambda_n H)^{-1}$$

$$B_n = \frac{1-(-1)^n}{n\lambda_n^2}$$

$$\lambda_n^2 = \frac{n^2\pi^2}{4} - \sigma_1$$

Figures 3-6 display representative features of the temperature fields for narrow-gap and wide-gap chambers. Figures 3 and 5 are perspective views, Figures 4 and 6 are sections. A noteworthy feature is that the effect of side walls, shown on Figures 4 and 6, persists for a distance of 2-3 half thicknesses into the chamber at each side. For the wide-gap chamber (0.5 cm wide) this distance is (roughly) 0.75 cm and for the narrow-gap chamber (0.15 cm wide), 0.45 cm. Thus, due to the effect of temperature, particles within these regions will have a different electrophoretic mobility from those in the interior. In addition, buoyancy effects will be accentuated.

FIGURE 3.

Perspective view of the temperature field for the narrow-gap chamber operating at conditions listed on Table I (uniform thermal conductivity). Note: 2d = 0.15 cm, 2h = 5 cm. Eq. (12).

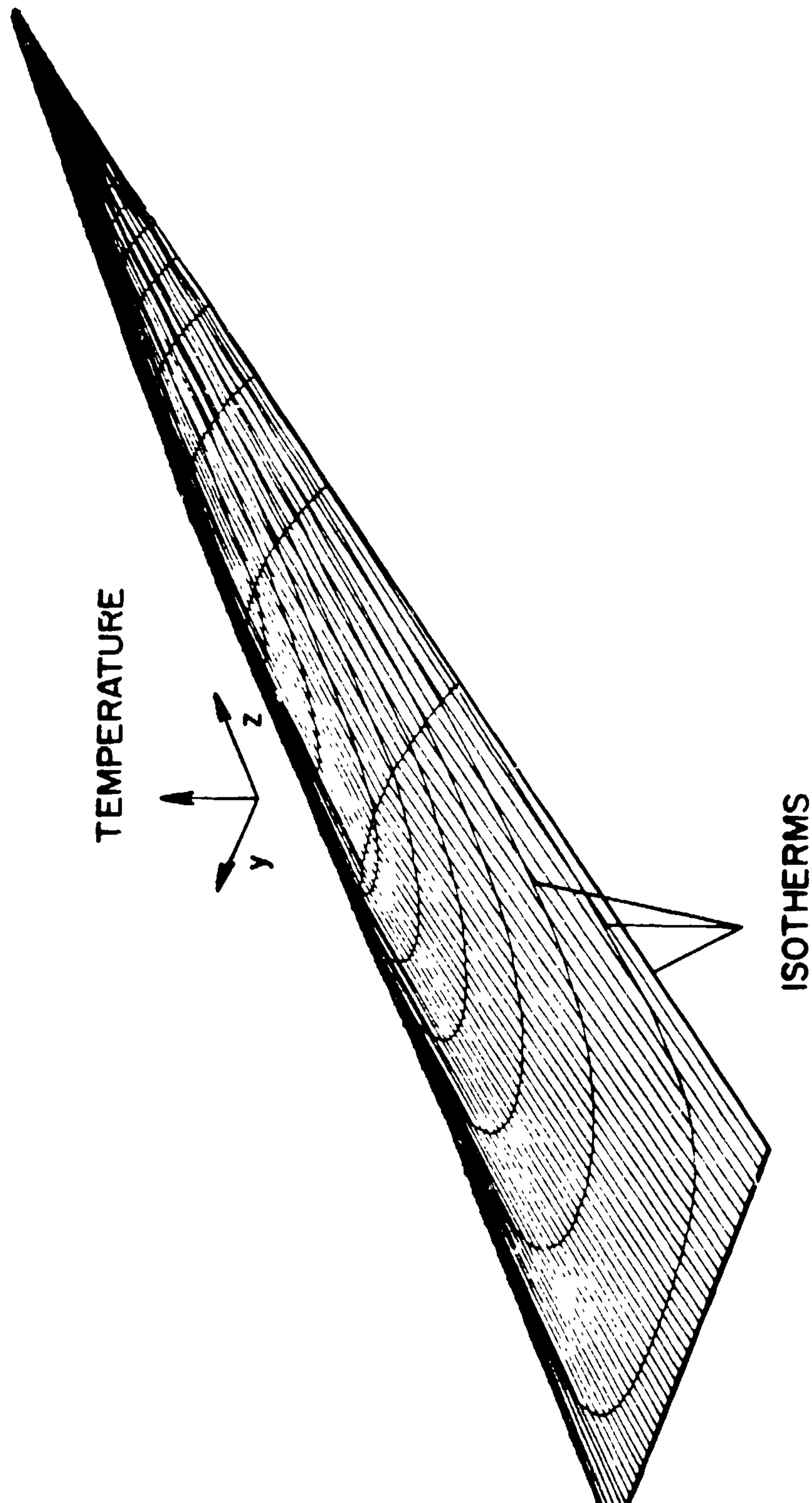
TEMPERATURE
z
y
ISOTHERMS

FIGURE 4.

Sections of the temperature field as shown in Figure 3.

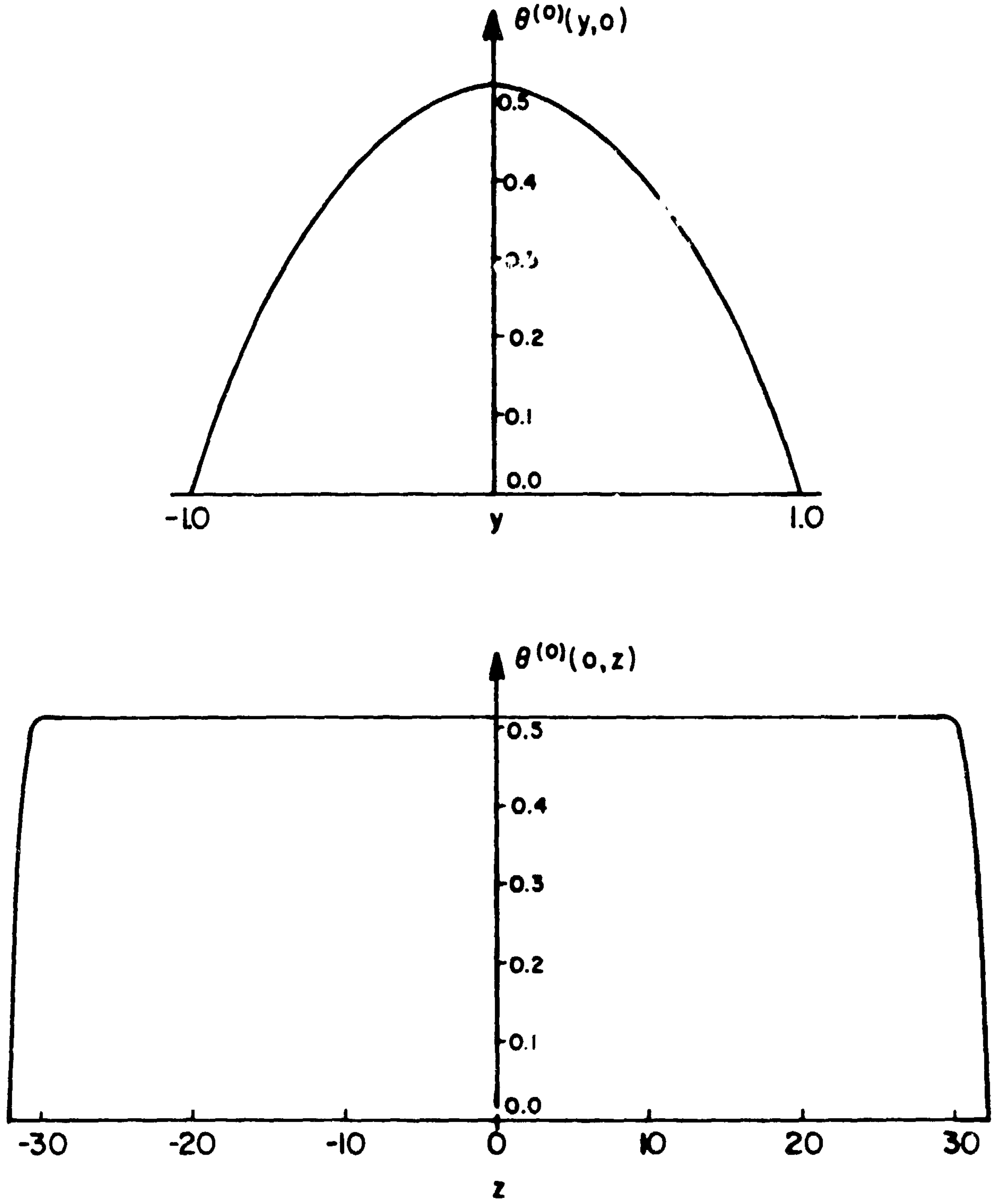
θ(0)(y,0)
0.5
0.4
0.2
0.1
0.0
-1.0
y
1.0
θ(0)(0,z)
0.5
0.4
0.3
0.2
0.1
0.0
-30
-20
-10
0
10
20
30
z

FIGURE 5.

Perspective view of the temperature field for the wide-gap chamber operating at conditions listed on Table I (iniform thermal conductivity). Note: 2d = 0.5 cm, 2h = 5 cm. Eq. (12).

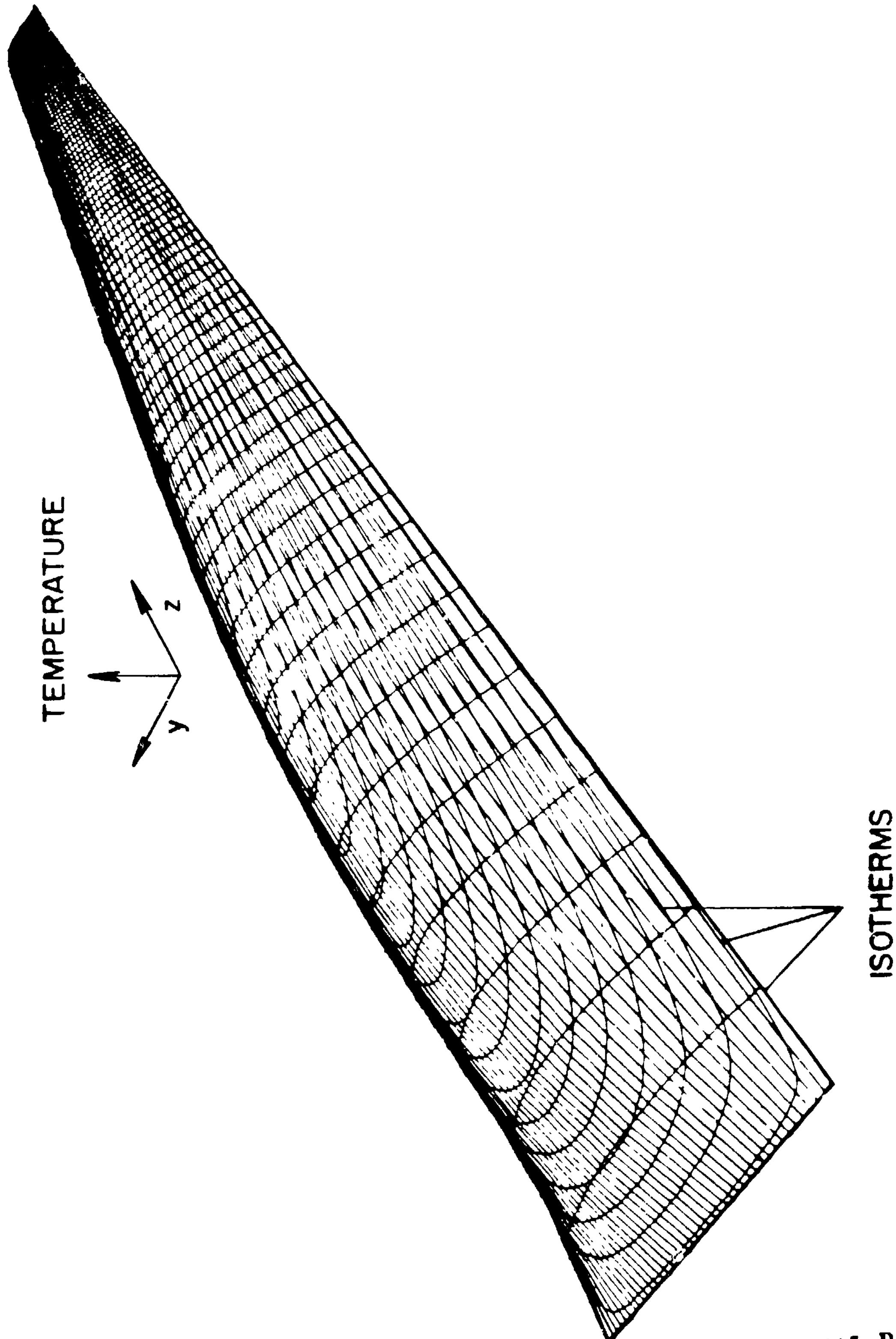
TEMPERATURE
z
y
ISOTHERMS

FIGURE 6.

Sections of the temperature field as shown in Figure 5.

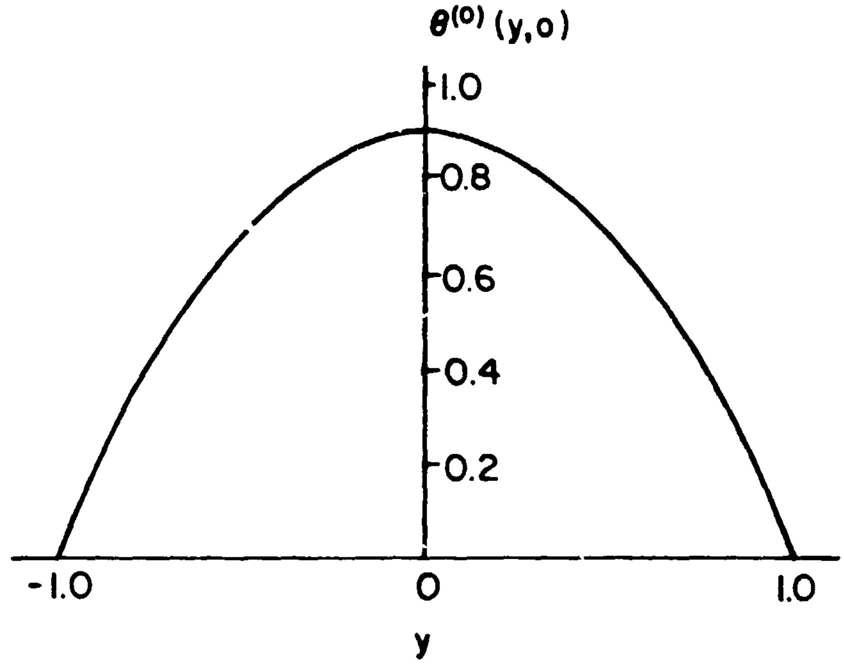
θ(0) (y,o)
1.0
0.8
0.6
0.4
0.2
-1.0
0
1.0
y

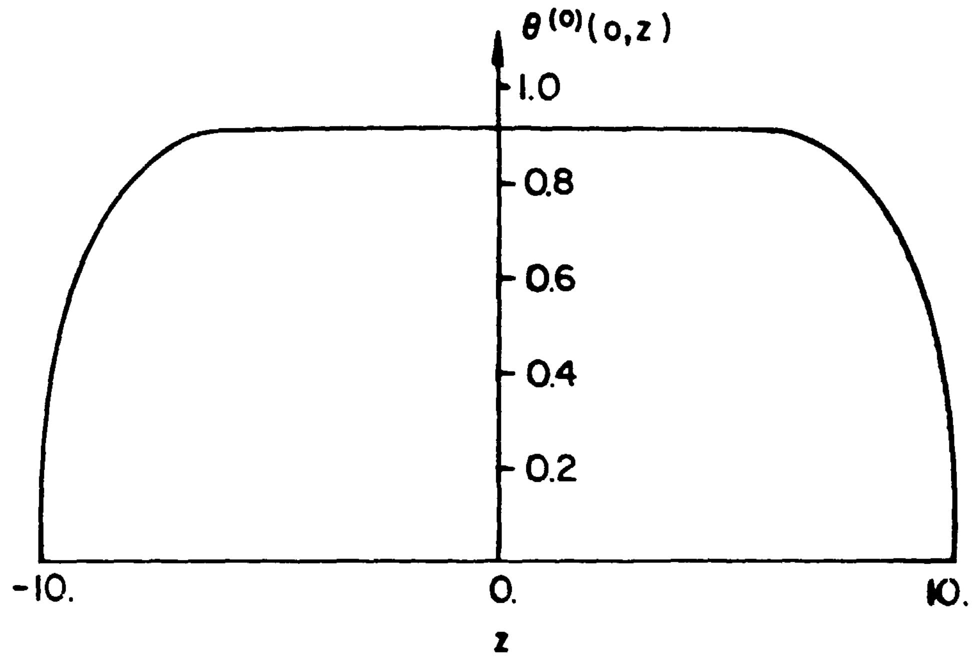
θ(0)(o,z)
1.0
0.8
0.6
0.4
0.2
-10.
0.
10.
z

One-Dimensional, Variable Thermal Conductivity Model

A one-dimensional temperature field corresponds to a very wide chamber, $H \rightarrow \infty$, or one with insulated end walls at $z = \pm H$. The zero-order field is given by

$$\theta^{(o)}(y) = \frac{1}{\sigma_1}\left[\frac{\cos N_1 y}{\cos N_1} - 1\right] \tag{13}$$

$$N_1^2 = \sigma_1$$

and perturbations are found from solutions to

$$\frac{d^2\theta^{(1)}}{dy^2} + \sigma_1\theta^{(1)} = -\frac{1}{2}\frac{d^2}{dy^2}\left[\theta^{(o)}\right]^2 \tag{14}$$

Using Fourier transforms the solution is found to be

$$\theta^{(1)}(y) = \frac{2}{\pi}\sum_{1}^{\infty} f_s(n)\sin\left[\frac{n\pi}{2}(1+y)\right] \tag{15}$$

where

$$f_s(n) = -\frac{1}{2}\frac{n^2}{n^2-4\sigma_1/\pi^2} S_n\{(\theta^{(o)})^2\}$$

$$Sn\{(\theta^{(o)})^2\} = \text{sine transform of } (\theta^{(o)}(y))^2.$$

Temperature fields for narrow-gap and wide-gap chambers are shown on Figure 7, along with that for constant thermal and electrical conductivities. Figure 7 depicts matters in dimensionless form and it is seen that with the wide gap the temperature rise is 1.7 times that expected with constant properties at the conditions shown, for the A-1 buffer this is nearly 30°C.

FIGURE 7.

One-dimensional temperature field calculated so as to account for temperature dependent thermal conductivity and electrical conductivity, A - wide-gap, B - narrow-gap, C - constant properties (cf. Table I). Eqs. (13) and (15).

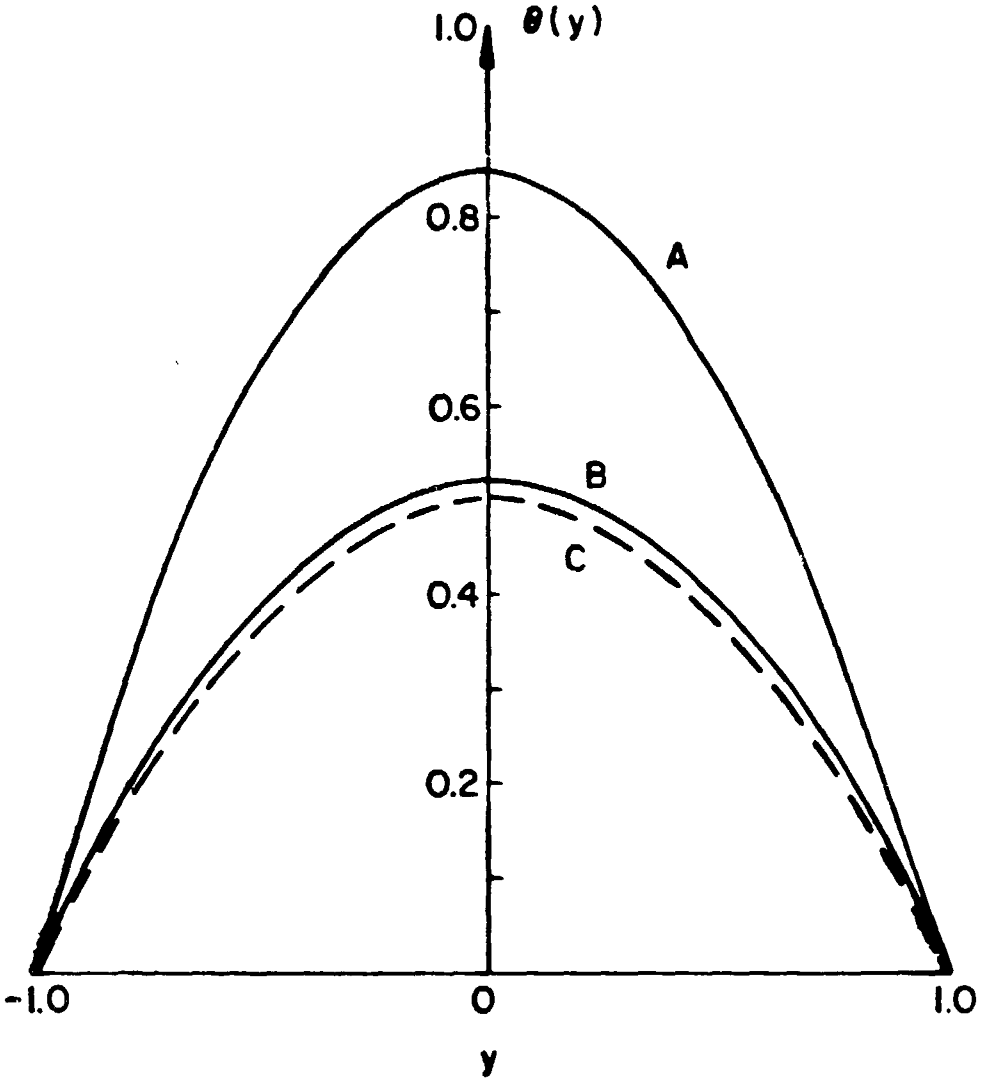
1.0
θ(y)
0.8
A
0.6
B
C
0.4
0.2
-1.0
0
1.0
y

With the narrow-gap, the temperature rise is so small, about 1.5°C, that variable-property effects are negligible. Here we also see (upon comparison with Figure 5) that the influence of variable thermal conductivity serves to alter the temperature rise. Accounting for the variable thermal conductivity lowers this maximum by about 2°C for the wide-gap chamber at the conditions shown.

One-Dimensional, Transient Response Model

An estimate of the minimum time required to reach a steady thermal state can be made using a transient thermal model which ignores convection, since it tends to increase the equilibration time by adding colder fluid and withdrawing warm fluid from the region of interest. A *rough* estimate can be found from the characteristic relaxation time scale, d^2/α_o. For the A-1 buffer $\alpha_o = 1.39$ cm^2/s so that for a narrow-gap machine (d = 0.075 cm) the time scale is about 4 seconds; for the wide-gap machine the time-scale is 45 seconds. To attain a condition near the steady-state generally requires 2-3 'relaxation times', as shown on Figures 8 and 9. Data for the graphs were calculated using the solution to a transient heat conduction problem with heat generation, viz.

$$\frac{\partial\Theta}{\partial\tau} = \frac{\partial^2\Theta}{\partial y^2} + 1 + \sigma_1\Theta \qquad (16)$$

with $\Theta(\tau,\pm 1) = 0$, $\Theta(0,y) = 0$. The solution given by Carslaw and Jaeger (1959) is

FIGURE 8.

Transient temperature response for a narrow-gap chamber (one-dimensional, constant thermal conductivity) (cf. Table I). Eq. (17).

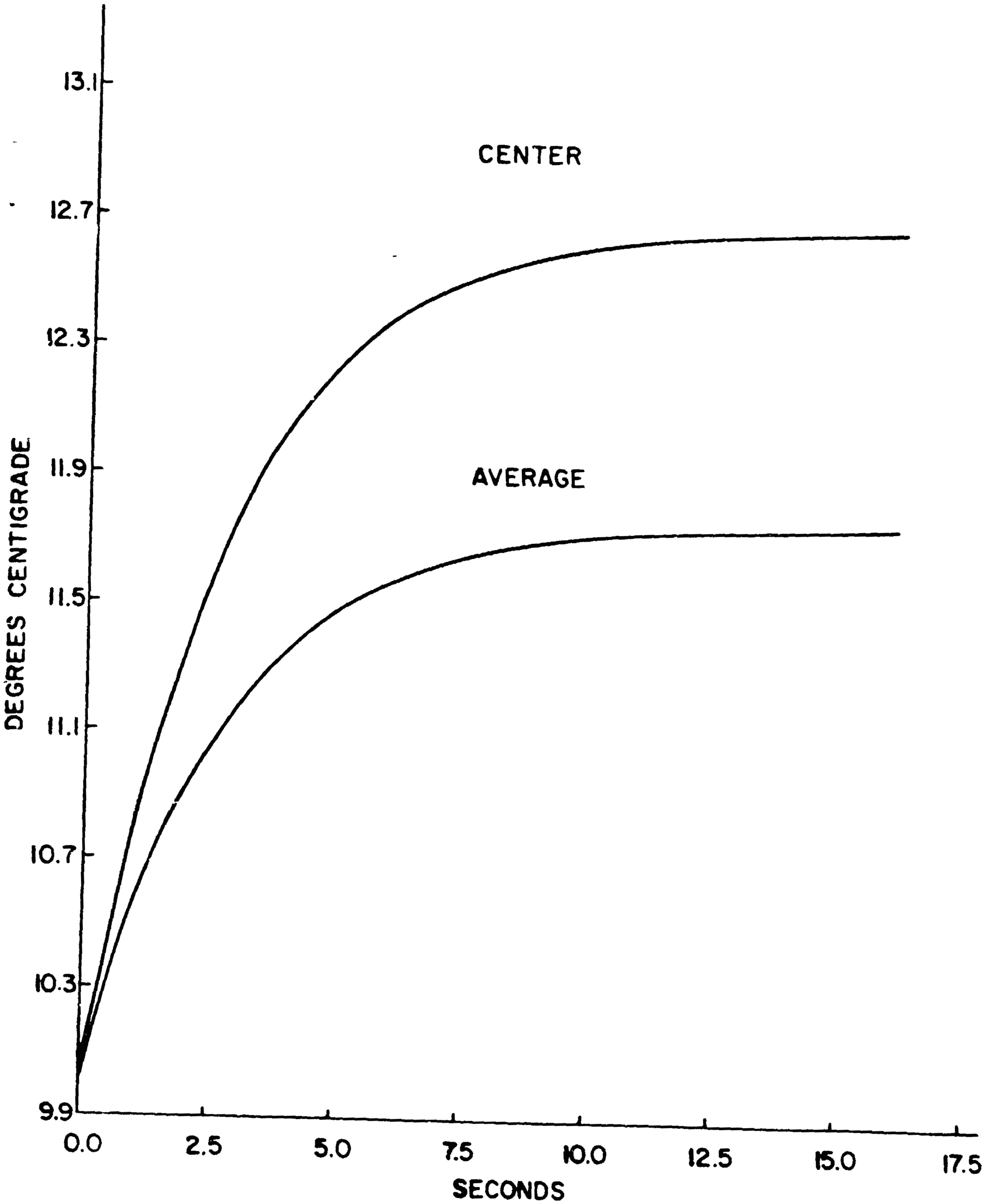
CENTER
AVERAGE
DEGREES CENTIGRADE
13.1
12.7
12.3
11.9
11.5
11.1
10.7
10.3
9.9
0.0
2.5
5.0
7.5
10.0
12.5
15.0
17.5
SECONDS

FIGURE 9.

Transient temperature response for a wide-gap chamber (one-dimensional, constant thermal conductivity) (cf. Table I). Eq. (17).

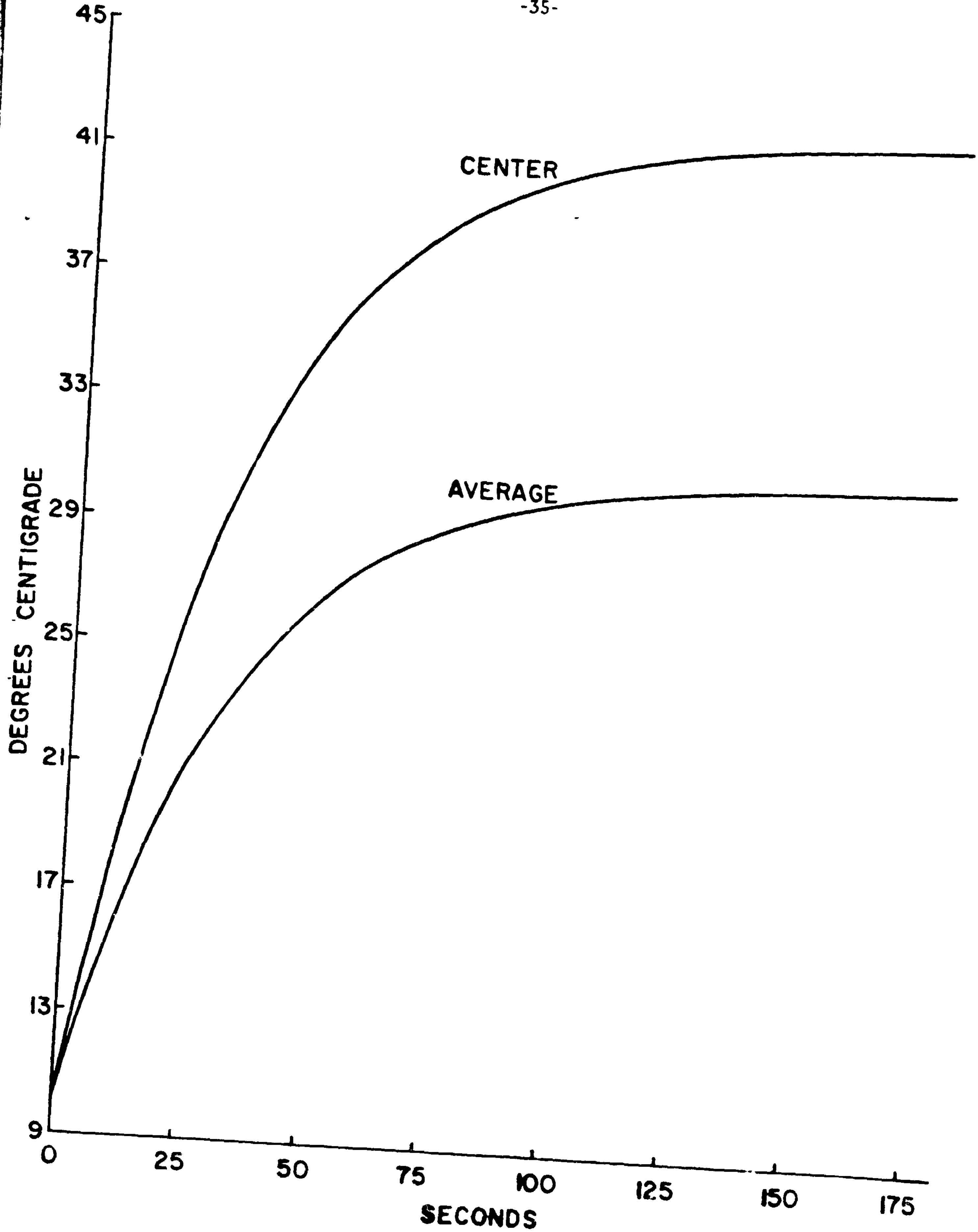
45
41
37
33
29
25
21
17
13
9
DEGREES CENTIGRADE
CENTER
AVERAGE
0
25
50
75
100
125
150
175
SECONDS

$$\Theta = \frac{1}{\sigma_1}\left[\frac{\cos N_1 y}{\cos N_1} - 1\right] + \frac{16}{\pi}\sum_{o}^{\infty}(-1)^n \frac{\exp(\cdot)\cos[2n+1)\pi y/2]}{[4\sigma_1-(2n+1)^2\pi^2][2n+1]}$$

$$(\cdot) = [-(2n+1)^2\pi^2+\sigma_1]\tau \tag{17}$$

$$\tau = \alpha_o t/4d^2, \quad y = y^*/d$$

Obviously a more refined estimate could be made by solving a two-dimensional with convection included, however, the characteristic time for equilibration would probably not change too much. Thus, in any experiment with wide-gap machine at least 2-3 minutes should be allowed for thermal equilibration.

Axial Velocity Field

Equations to describe the axial velocity are derived from the Navier-Stokes equations using an expansion described earlier

$$u(y,z) = u^{(o)}(y,z) + u^{(1)}(y,z) + \ldots \tag{10}$$

The effects of buoyancy on the two-dimensional flow field are described in the first part of this section. In the second, where the effects of the lateral boundaries at $z = \pm H$ are ignored, exact solutions are possible which account fully for the effects of temperature on viscosity and buoyancy.

Two-Dimensional, Constant Transport Properties Model

The 0(1)-velocity is described by solutions to

$$0 = - K + N_2 - N_3\Theta^{(o)} + \nabla^2 u^{(o)} \qquad (18)$$

where K is a constant (dimensionless) axial pressure gradient; $N_2 = gd^3/\nu_o^2$ Re and $N_3 = gd^3\beta\Delta T/\nu_o^2$ Re, Re = du_o/ν_o. The parameter N_3 describes the magnitude of the buoyancy effect while $(-K + N_2)$ is a constant to be determined from the fact that the volumetric flowrate is independent of the temperature rise, since the velocity is scaled using the mean velocity, u_o. Using Fourier Sine transforms we find

$$u^{(o)}(y,z) = \frac{2}{\pi}\sum_{o}^{\infty} g_s(n)\sin\frac{n\pi}{2}(1+y) \qquad (19)$$

with

$$g_s(n) = B_n\cosh\frac{n\pi}{2}z + C_n\cosh\lambda_n z + D_n$$

The coefficients B_n, C_n, and D_n are found from the relations

$$B_n\cosh\frac{n\pi H}{2} + C_n\cosh\lambda_n H + D_n = 0$$

$$C_n = -\frac{N_3A_n}{\sigma_1}$$

$$D_n = -\frac{4}{n^2\pi^2}\left[\frac{K-N_2}{n}(1-(-1)^n) + \frac{N_3}{n}\frac{(1-(-1)^n)}{\lambda_n^2}\right] \qquad (20)$$

Finally $(-K + N_2)$ is found from the requirement that

$$\int_{-H}^{H}\int_{-1}^{1} u^{(o)}(y,z)\,dy\,dz = 4H \qquad (21)$$

FIGURE 10.

Axial velocity field for the narrow-gap chamber (cf. Table I). The velocity is almost indistinguishable from the fully developed parabola, $3(1-y^2)/2$ except near the side walls at $z = \pm 33.3$. Eq. (19).

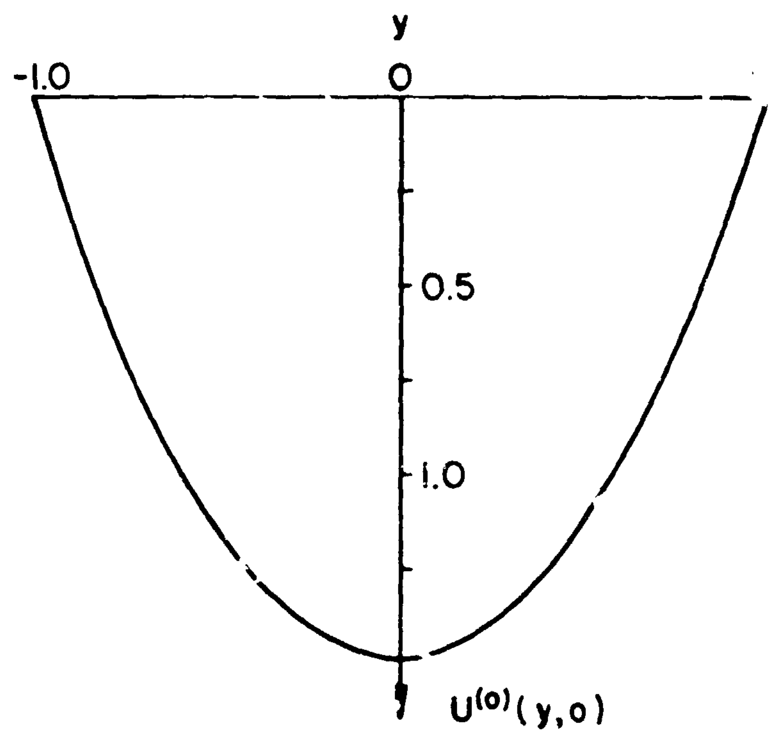

10

FIGURE 11.

Perspective view of the axial velocity field for the wide-gap chamber (cf. Table I). Downflow at $g = 980$ cm/s^2. Eq. (19).

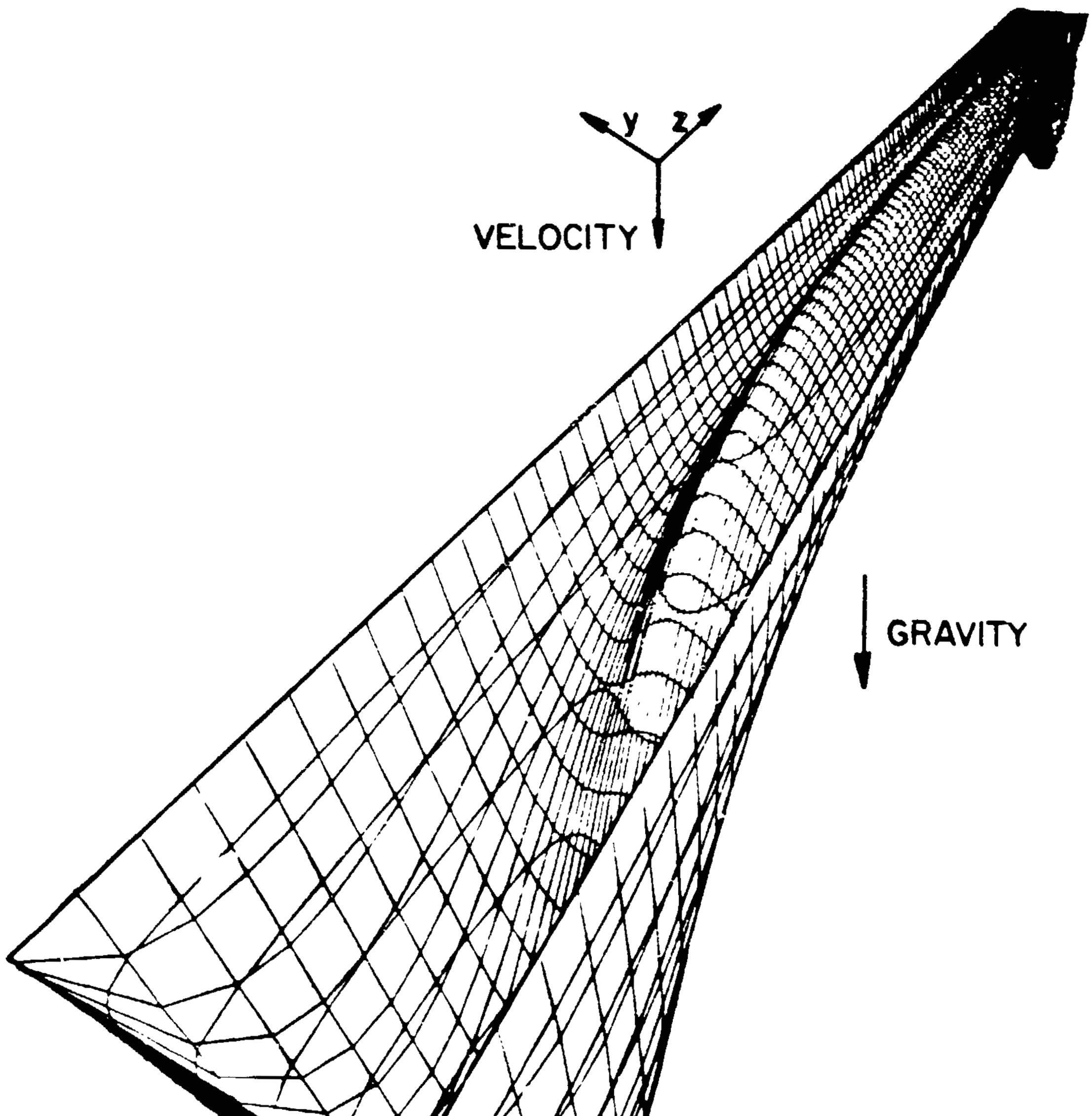
y
z
VELOCITY
GRAVITY

FIGURE 12.

Central sections of the field shown on Figure 11. Note weak upflow in center and strong downflow along front and back cooling walls and near side walls at $z = \pm 10$.

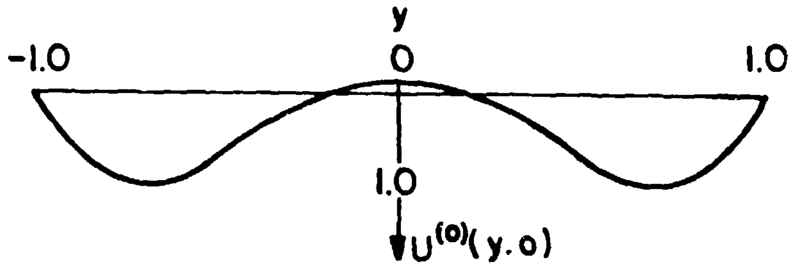

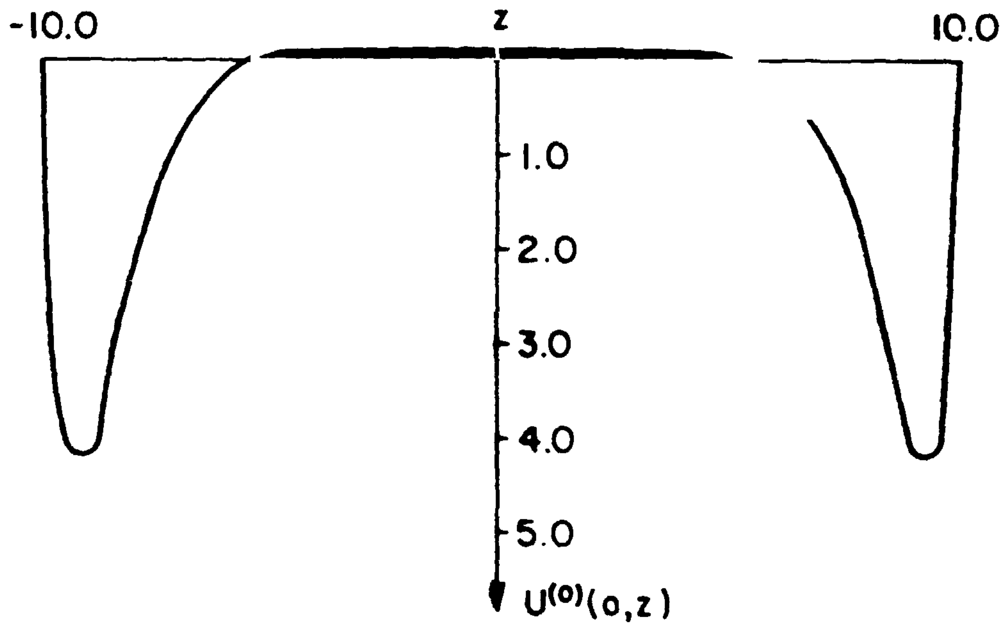

DIRECTION OF MAIN FLOW AND GRAVITY

FIGURE 13.

Perspective view of the axial velocity field for the wide-gap chamber (cf. Table I). Upflow at $g = 980\ cm/s^2$. Eq. (19).

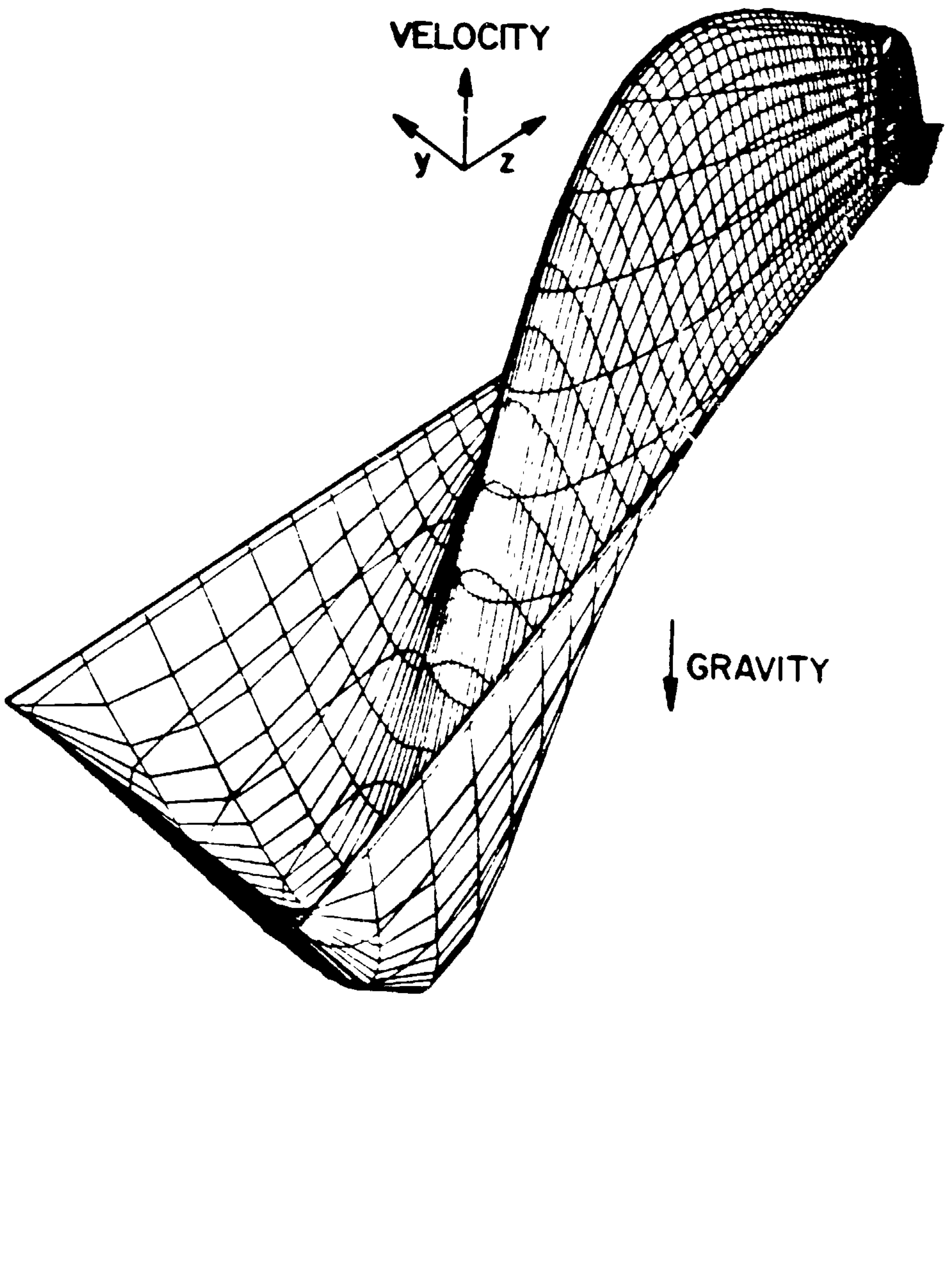
VELOCITY
y
z
GRAVITY

FIGURE 14.

Central sections of the field shown on Figure 13. Note downflow along front and rear cooling walls and near the side walls at $z = \pm 10$.

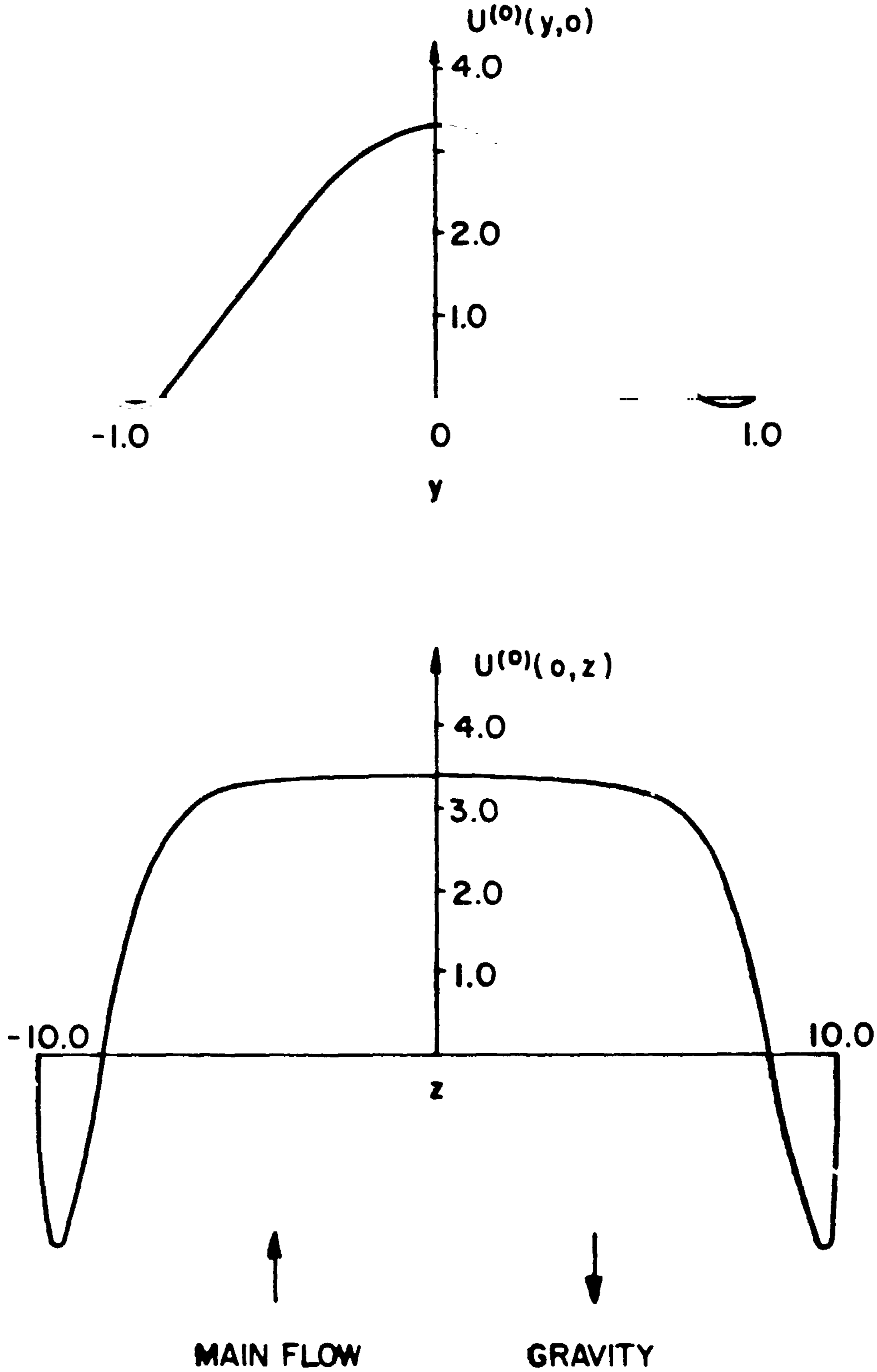
U(0)(y,o)
4.0
2.0
1.0
-1.0
0
1.0
y
U(0)(o,z)
4.0
3.0
2.0
1.0
-10.0
10.0
z
MAIN FLOW
GRAVITY

Results of representative calculations are shown on Figures 10-14 Figure 10 shows that buoyancy has relatively little effect on a narrow-gap chamber due to the excellent heat transfer. The maximum temperature rise for this case is about 1°C. End effects due to the no-slip condition at $z = \pm H$ are similar to those encountered with the temperature field.

With the wide-gap chamber dramatic effects are present at unit gravity. Figure 11 is a perspective view, Figure 12 shows the velocity across two sections of the chamber with downflow. Here buoyancy causes regions of reversed flow throughout a large part of the central section. With a finite length chamber this implies that a large recirculating eddy would be present in the central section and the chamber would be difficult to use as an electrophoretic separation device. If the flow is reversed, the recirculating eddy splits apart and is attached to the side walls, as is shown on Figures 13 and 14. Since the recirculating regions are adjacent to the side walls, the central section allows more-or-less free passage of fluid and any sample. Of course, any sample that migrated into the eddy structures would be difficult to recover.

One-Dimensional Velocity Fields

Effects due to a temperature dependent viscosity and buoyancy can be investigated easily using a one-dimensional model and, in fact, exact solutions can be obtained. Since variations are confined to the y-direction we have

$$0 = K + N_2\rho + \frac{d}{dy} \mu \frac{du}{cy} \quad (22)$$

with

$$u(\pm 1) = 0$$

The solution is

$$u(y) = -K\int_y^1 \frac{y_1}{\mu}\,dy_1 + N_2\int_y^1 \frac{1}{\mu}\int_0^{y_2} \rho\, dy_1 dy_2 \qquad (23)$$

with K determined from the fact that the velocity scale is the mean velocity. Thus

$$1 = -K\int_0^1\int_y^1 \frac{y_1}{\mu}\,dy_1 dy + N_2\int_0^1\int_y^1 \frac{1}{\mu}\int_0^{y_2} \rho\, dy_1 dy_2 dy \qquad (24)$$

Given expressions for the dimensionless viscosity, and density, both scaled on values evaluated at the wall, it is a straightforward task to evaluate the integrals. In the calculation a two-term expression was used for the temperature, viz.

$$\Theta = \Theta^{(o)} + k_1\Theta^{(1)} \qquad (7)$$

For purposes of comparison we can evaluate the velocity field for uniform viscosity and buoyancy. The temperature field is

$$\theta^{(o)}(y) = \frac{1}{\sigma_1}\left[\frac{\cos N_1 y}{\cos N_1} - 1\right], \quad N_1^2 = \sigma_1 \qquad (13)$$

and the velocity works out to be

$$u^{(o)}(y) = \frac{3}{2}(1-y^2) - \frac{3N_3}{\sigma_1}\left[\frac{1}{\sigma_1} + \frac{1}{3} - \frac{1}{\sigma_1 N_1}\tan N_1\right](1-y^2)$$
$$+ \frac{N_3}{\sigma_1}\left[\frac{1}{\sigma_1} + \frac{1}{2}(1-y^2) - \frac{1}{\sigma_1}\frac{\cos N_1 y}{\cos N_1}\right] \qquad (25)$$

For $\sigma_1 \rightarrow 0$ we recover an earlier result due to Ostrach (1976),

$$u^{(o)}(y) = \frac{3}{2}(1-y^2) - \frac{N_3}{120}(1-y^2)(1-5y^2) \qquad (26)$$

It is important to note that the magnitude of the buoyancy effect as compared to forced convection is contained in the dimensionless group N_3, viz.

$$\frac{g\beta}{\nu_o u_o} \frac{\sigma_o E_o^2 d^4}{k_o} .$$

Here β represents an average coefficient of thermal expansion, $-\rho^{-1}(\partial\rho/\partial T)$. Thus, all other things being equal, going from a narrow-gap machine (2d = 0.15 cm) to a wide-gap machine (2d = 0.5 cm) alters the effect of gravity by a factor of $(10/3)^4$, roughly two orders-of-magnitude. It follows that whereas gravity forces play minor roles with narrow-gap machines the situation with wide-gap machines is quite the opposite.

For $|N_3| << 1$ the velocity differs very little from the familiar parabolic profile characteristic of forced convection. For $|N_3| >> 1$ regions of reverse flow are present as illustrated on Figures 15 and 16. Qualitatively these profiles are similar to those derived from the two-dimensional model; quantitatively, however, they differ in the magnitude of the maximum velocity, which is higher here due to the effects of variable viscosity and buoyancy. Note regions of reversed flow in the center for downflow and adjacent to side walls for upflow (see insets).

The recirculating eddy present in the downflow configuration at *these operating conditions* renders this configuration almost useless for electrophoretic separation. Even if the flow was steady, the sample stream would be deflected towards the wall where electro-osmotic effects would be strong.

FIGURE 15.

One-dimensional velocity field calculated with allowance for variable viscosity and density (cf. Table I). Downflow, g = 980 cm/s^2. Eq. (23).

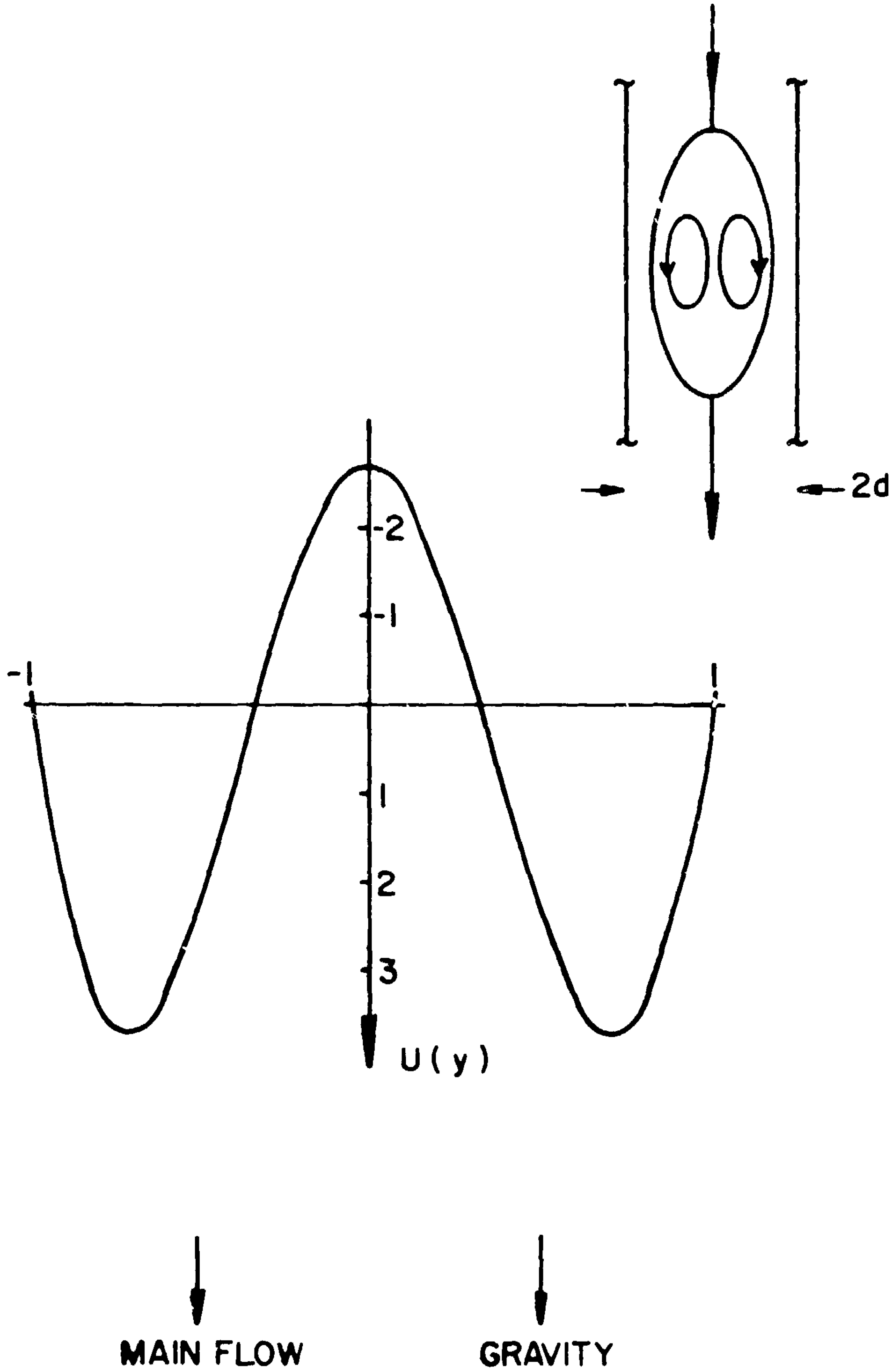
2d
-1
1
-2
-1
1
2
3
U (y)
MAIN FLOW
GRAVITY

FIGURE 16.

One-dimensional velocity field calculated with allowance for variable viscosity and density (cf. Table I). Upflow, $g = 980$ cm/s^2. Eq. (23).

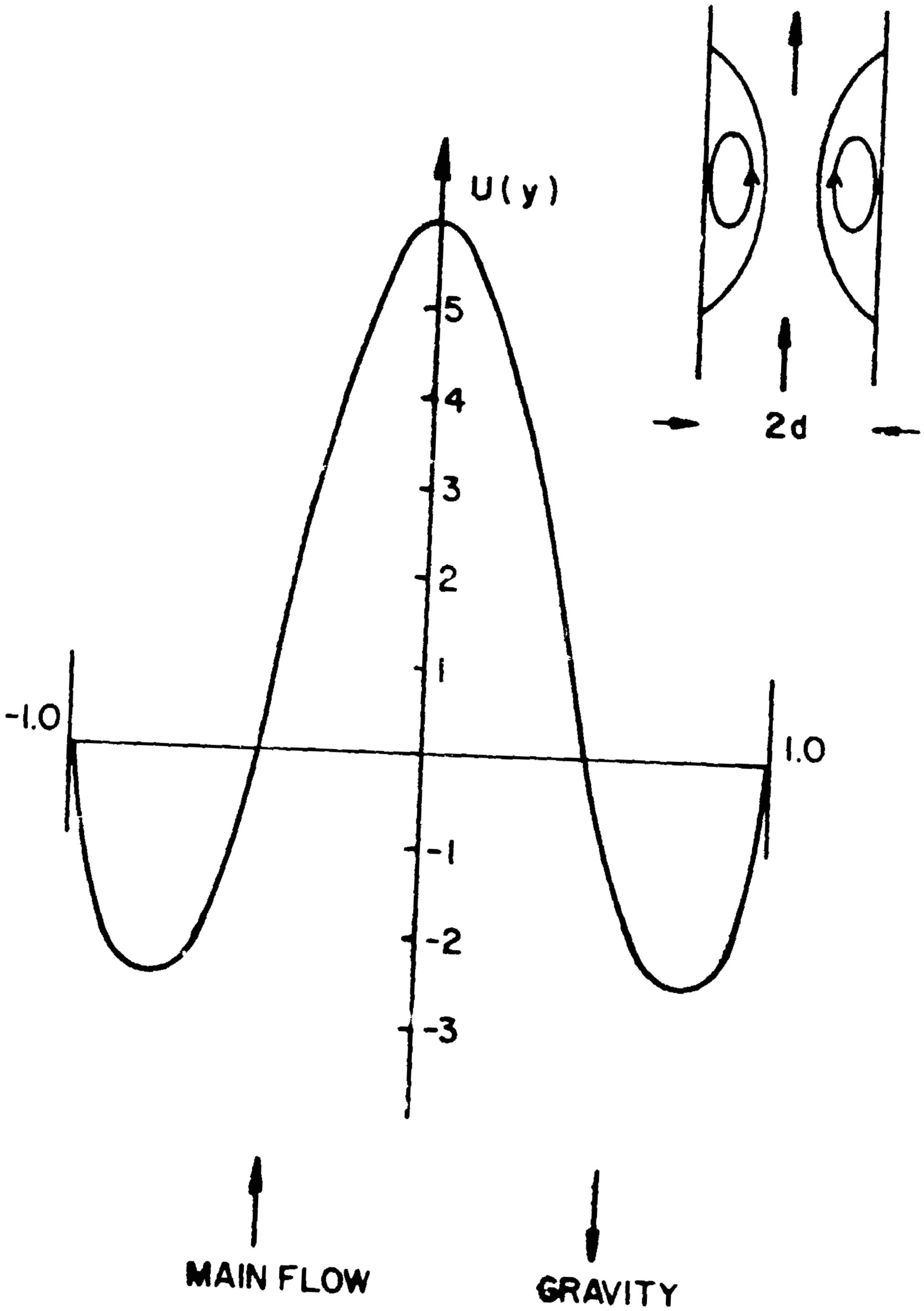

16

In the upflow configuration the eddys attached to the walls take up nearly 80% of the cross section and severely reduce the region available for sample separation.

At the same time, however, it must be recognized that the calculations presented here do not exhaust the set of configurations and operating conditions. The recirculations, for example, can be changed by independent control of the pressure gradient. Lowering the field strength has a dramatic effect on the buoyancy, since the temperature rise is proportional to E_o^2, but would necessitate an increase in the length of the chamber, etc. There are, therefore, a number of options which remain to be investigated, the calculations given here simply illustrate the hydrodynamic phenomena.

Electro-osmotic Cross-flow Velocity Field

The presence of a thin layer of space charge adjacent to the boundaries in the y-z plane (cf. Figure 1) along with the transverse electric field causes a well-known electro-osmotic flow (Shaw, 1969). In a parallel plate system open to reservoirs at $z = \pm H$ where $H >> 1$ the velocity profile would appear to be flat up to a very small distance from the wall (a few multiples) of the Debye thickness, κ^{-1}) where a rapid transition occurs to accommodate the no-slip condition. For most purposes the double-layer thickness, κ^{-1} is so small that we can approximate the velocity just outside this layer using one of the Smoluchowski equations,

$$w_o = - \varepsilon E_o \zeta / \mu \tag{27}$$

where w_o is the velocity in the z-direction, ε, the dielectric constant, E_o, the field strength and, ζ, the zeta-potential of the wall material in contact with the solution in question. This apparent slip-velocity is of the order of a few microns per second for a potential gradient of one volt per centimeter. When the flow is constrained by walls at $z = \pm H$ the profile is forced to be (roughly) parabolic so as to accommodate the condition of no net flow across the y-z plane. Although this velocity is too slow to affect the axial flow substantially the cross-flow interferes with any electrophoretic separation by stretching the sample cross section. To provide an estimate of thermal effects and furnish a consistent representation of the velocity field for use in the separations model a simplified model is used. In this model end effects are omitted except insofar as the walls force the flow to turn round as sketched in Figure 17. The electro-osmotic velocity can be calculated from solutions to

$$0 = -\frac{\partial p}{\partial z} + \frac{\partial}{\partial y}\mu\frac{\partial w}{\partial y} \tag{28}$$

with $w = w_o$ at $y = \pm d$.

The pressure gradient arises from the need to balance viscous forces outside the double-layer so as to produce a field with no net flow. If we scale the velocity using w_o, and lengths using d, and write the viscosity as $\mu_o\mu(\theta)$ to account for the thermal effects we obtain

$$0 = K_2 + \frac{d}{dy}\mu\frac{dw}{dy} \tag{29}$$

which can be integrated to

$$w = K_2\int_1^y \frac{y_1}{\mu}\,dy_1 - 1 \tag{30}$$

The constant K_2 is found from the requirement that the net flow across any cross section in the x-y plane be zero.

Although effects due to temperature dependent viscosity are relatively small and change the velocity only about 10% in the wide-gap chamber, these could be significant if one were modelling the separation of particles with small mobility differences.

FIGURE 17.

Electro-osmotic crossflow velocity: A - plan view showing recirculation caused by end walls, B - velocity profile with constant viscosity, $(1 - 3y^2)/2$; C - velocity profile with wide-gap (cf. Table I).

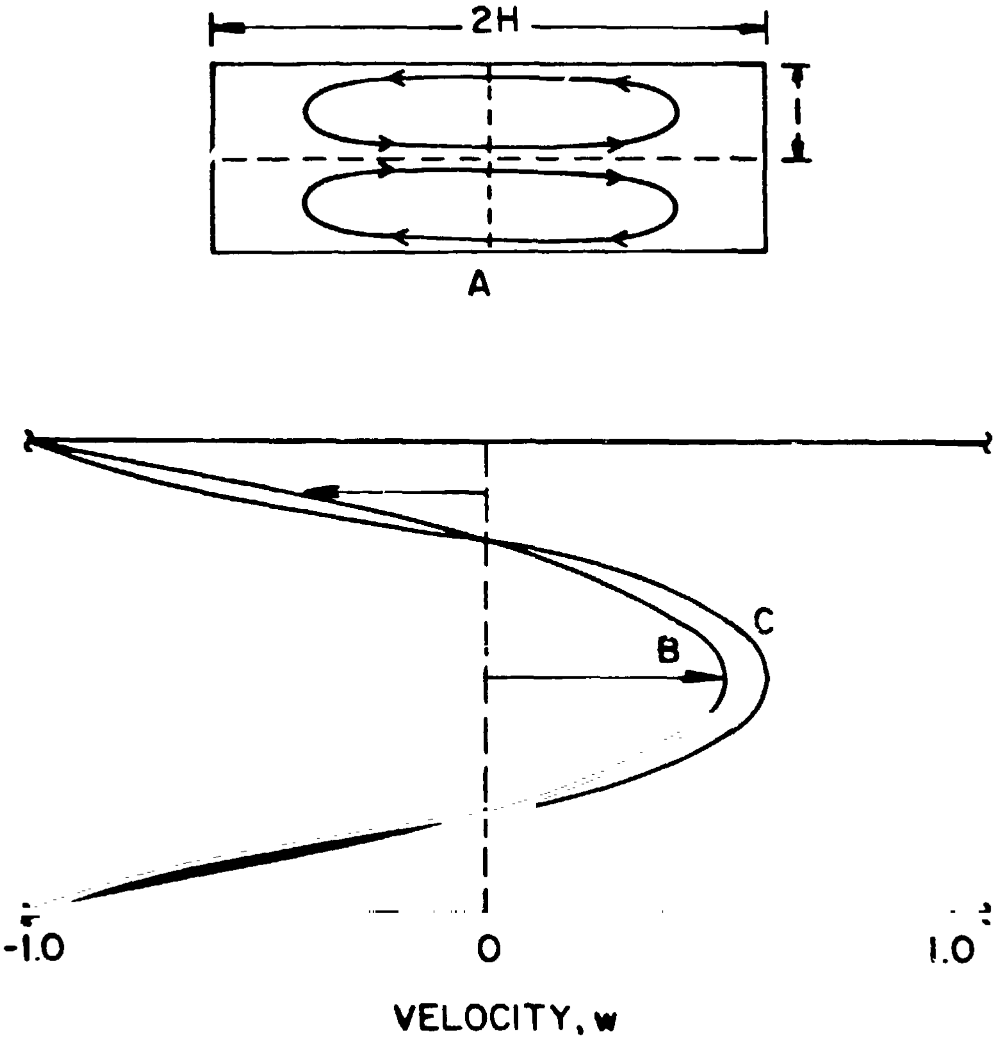
2H
A
B
C
-1.0
0
1.0
VELOCITY, w

II. HYDRODYNAMIC STABILITY

Introduction

During the early s· ·ges of development of the wide-gap machines large scale, irregular convective mixing was observed during experiments with dye tracers. One of the possible causes is the flow reversal caused by buoyancy (see Part I and Ostrach, 1976). At that time, the absence of quantitative data prevented a rest of this hypothesis. Later experiments at General Electric by H. Semon (1977) provided additional data and disclosed a persistent "wavering" of the sample stream at low power inputs; higher power levels caused irregular mixing. However, the power levels corresponded to maximum (centerline) temperatures only a few degrees higher than the wall (buffer) temperature, far below those which could produce the w-shaped profiles described in Part I. According to the analysis in Section I the dimensionless group $g\beta\sigma_o E_o^2 d^4/\nu_o k_o u_o$ must be $0(10^2)$ or more for buoyancy to alter the velocity profile significantly; in the General Electric experiments it was 0(1). Changes in the orientation of the flow relative to gravity changed the allowable power levels somewhat but irregular flow persisted at voltage gradients necessary to give a significant electrophoretic separation. It was decided, therefore, to investigate the hydrodynamic stability of the flow.

Several sorts of phenomena are included under the general topic of hydrodynamic stability: the inception of motion in an otherwise quiescent system, the transition from one steady laminar flow to another and transition from laminar to turbulent flow. To establish orders-of-magnitude, theories for the stability of a horizontal layer and of a shear flow were reviewed. As a result it appears that neither of the buoyancy mechanisms involved in these

ORIGINAL PAGE IS
OF POOR QUALITY

two situations would be able to destabilize the flow.

Previous work on the stability of stratified fluid layers has centered on quiescent layers (cf. Chandrasekhar, 1961; Ostrach, 1964). This body of literature was combed to locate reports of special significance to the problem at hand which is distinguished by the combined processes of volumetric heat generation and fluid motion. Sparrow, Goldstein and Jonsson (1964) studied the buoyancy driven instability of a quiescent, horizontal layer bounded above and below by rigid walls and heated internally. Although a nonlinear profile does lower the critical temperature difference considerably, calculations based on parameter values for the wide-gap chamber showed that the critical difference is about 10°C which is well above the values reported by General Electric for the horizontal (or vertical) configuration with flow. Allowance for the effect of temperature on the rate of heat generation (which is not part of the Sparrow-Goldstein-Jonsson theory) may lower the critical temperature difference somewhat but an extension of this sort was not attempted, since it seemed best to understand the behavior of the vertical configuration which would be used in electrophoretic separation.

Vest and Arpaci (1969) studied the stability of natural convection in a vertical slot, where however, since the base flow is driven by an anti-symmetric temperature, it is different from that in a continuous flow electrophoresis chamber. The stability with respect to roll waves, oriented perpendicular to the main flow was examined and a critical Grashof number of 7880 was found for this sort of instability. In the General Electric experiment the Grashof number based on the maximum centerline temperature is roughly 10 and, although the circumstances are quite dissimilar, it seems unlikely that the observed meandering derives from a shear instability of the sort studied by Vest and Arpaci.

If the meandering and subsequent large scale convection are the result of an instability, then it must be one where the critical Rayleigh number is small. One possibility is that the instability derives from small *axial* temperature gradients which result from uneven heating or cooling. In addition the thermal region near the entrance to the electrode section extends over a region of several chamber half-thicknesses. This gradient can be estimated from an earlier equation describing the balance between convection, conduction and generation,

$$\mathrm{Pe}\ u(y)\ \frac{\partial\Theta^{(o)}}{\partial x} = \frac{\partial^2\Theta^{(o)}}{\partial y^2} + 1 + \sigma_1\Theta^{(o)} \tag{8}$$

for temperature-independent properties. This equation has solutions which decay exponentially with x and have the form

$$e^{-\lambda_n^2\, x\, \mathrm{Pe}^{-1}}\ f_n(y)$$

The mode which has the smallest eigenvalue, λ_n, fixes the relaxation distance, x_e. An estimate of the smallest eigenvalue can be found from the problem where the variable velocity u(y) is approximated by the (constant) average velocity. A more exact calculation would refine this estimate but would not change the order-of-magnitude. It is found that the distance over which the temperature adjusts to the ohmic heating is approximately (Pe)(d). For the wide-gap chamber operation at the conditions listed on Table I the Peclet number is about 50. Thus, since the temperature rise here is over 30 degrees, axial gradients at the inlet (and outlet) are of the order of 1°C/cm.

Stability of a Fully Developed Flow with an Axial Temperature Gradient

The presence of cold fluid above warmer fluid (in the region above the electrodes with the downflow configuration and in the electrode "outlet" region with upflow) is an unstable configuration. To study the stability of the velocity and temperature fields they were modelled with a fully developed axial flow in a rectangular channel. The basic temperature field consists of an axial gradient of magnitude denoted by A, with lateral variations due to the balance between heat generation and conduction through the walls, i.e.,

$$T = T_w + Ax + \Delta T \Theta(y,z) \qquad (31)$$

If we scale lengths, velocities, etc., as before we obtain

$$\frac{\partial u}{\partial \tau} = -\frac{\partial p}{\partial x} + N_2(1-\beta\Delta T) - \frac{Ra}{Pr\ Re}x - \frac{Gr}{Re}\Theta + \nabla^2 u \qquad (32)$$

$$Pr\frac{\partial \Theta}{\partial \tau} + \frac{Ra\ Re}{Gr}u = \nabla^2\Theta + 1 \qquad (33)$$

where

$Gr = g\beta\Delta T d^3/\nu_o^2$ Grashof number

$Ra = g\beta A d^4/\nu_o\alpha_o$ Rayleigh number

$Re = u_o d/\nu_o$ Reynolds number

$Pr = \nu_o/\alpha_o$ Prandtl number

with $u = \Theta = 0$ on boundaries at $y = \pm 1$, $z = \pm H$.

The mathematical problem is to identify conditions under which temperature and velocity fields other than the steady-state, symmetric forms exist. In particular we are interested in forms with an exponential time dependence, $e^{\omega t}$. The demarcation between stable and unstable flows is $\omega = 0$. Because of the linear structure of the equations we can show that the imaginary part of ω, $I_m(\omega)$, is zero so that the so-called "exchange of stabilities" principle is satisfied and any disturbance will grow exponentially. Thus, we simply look for conditions where $\omega = 0$. The problem is decomposed into the sum of the steady parts u, Θ and perturbations $\hat{u}$ and $\hat{\Theta}$.

This problem is very similar to one solved earlier by Ostrach (1955). Here those results are extended to include two-dimensional effects and other disturbance planforms. In the early work the instability was identified through a degeneracy in a base flow, now we see that the disturbances are superimposed on a symmetric base flow.

For the disturbance flow, $\hat{u}$, and temperature, $\hat{\Theta}$, we have

$$\nabla^4_{II}\hat{u} = Ra\,\hat{u}$$
$$\hat{\Theta} = Ra^{-1}\nabla^2_{II}u \qquad (34)$$

where ∇^2_{II} stands for the two-dimensional Laplace operator. $\hat{u} = \hat{\Theta} = 0$ on the boundaries. One set of solutions will, of course, simply be multiples of the symmetric (with respect to the x-z and x-y planes) steady-state solutions. We are interested in anti-symmetric solutions, which represent no change in the volumetric flow rate through the y-z plane. In general, the solutions to these equations can be written

$$\hat{u} = u_1 + u_2 \tag{35}$$

where

$$\nabla_{II}^2 u_1 = \lambda^2 u_1 \tag{36}$$

$$\nabla_{II}^2 u_2 = -\lambda^2 u_2$$

$$\lambda^4 = Ra$$

The temperature is

$$\Theta = Ra^{-1/2}(u_1 - u_2), \tag{37}$$

Solutions are

$$u_1 = \sin qz(A_1 \sinh \gamma_1 y + B_1 \cosh \gamma_1 y)$$

$$+ \cos qz(A_2 \sinh \gamma_1 y + B_2 \cosh \gamma_2 y)$$

$$\gamma_1^2 = q^2 + \lambda^2 \tag{38}$$

$$u_2 = \sin qz(A_3 \sinh \gamma_2 y + B_3 \cosh \gamma_2 y)$$

$$+ \cos qz(A_4 \sinh \gamma_2 y + B_4 \cosh \gamma_2 y)$$

$$\gamma_2^2 = q^2 - \lambda^2$$

To satisfy the boundary conditions on the walls at $z = \pm H$ either

$$\text{(i)} \quad \sin qH = 0, \; A_2 = B_2 = A_4 = B_4 = 0, \quad q = n\pi/H \; ; \tag{39}$$

or

$$\text{(ii)} \quad \cos qH = 0, \; A_1 = B_1 = A_3 = B_3 = 0, \quad q = \frac{2n-1}{2}\frac{\pi}{H} \; . \tag{40}$$

The first condition, (i), corresponds to a disturbance that is anti-symmetric with respect to the x-y plane with upflow on one side and downflow on the other. This form preserves the volumetric flow rate. The second condition, (ii), describes a flow with the requisite asymmetry if $B_2 = B_4 = 0$.

Next, with (i), either $B_1 = B_3 = 0$ so that $A_3 = 0$ and $\gamma_1 = \pm in\pi$ which gives

$$\lambda^4 = n^4\pi^4(1 + H^{-2})^2 \tag{41}$$

or $A_1 = A_3 = 0$ so that $B_3 = 0$ and $\gamma_1 = i(2n - 1)\pi/2$ which gives

$$\lambda^4 = \pi^4[(2n - 1)^2/4 + n^2/H^2]^2 \tag{42}$$

With (ii), $A_4 = 0$ and $\gamma_2 = \pm in\pi$ so that

$$\lambda^4 = \pi^4[n^2 + (2n-1)^2/4H^2]^2 \tag{43}$$

The mode with the lowest critical Rayleigh number corresponds to the velocity field

$$u_1 = \sin\frac{\pi z}{H}\cos\frac{\pi y}{2} \tag{44}$$

with the critical Rayleigh number

$$Ra_c = \frac{\pi^4}{16}(1 + H^{-2})^2 \tag{45}$$

For the wide-gap chamber with dimensions noted on Table I, $Ra_c = 6.58$ and with a narrow-gap, $Ra_c = 6.11$. Using data for water at 10°C the critical temperature gradient is 0.5°C/cm for the wide-gap and 53°C/cm for the narrow-gap chambers. These results agree *qualitatively* with experimental observation in that they disclose a great deal of sensitivity to axial temperature gradients for the wide-gap machine. With a narrow-gap it would be rather difficult to achieve the axial gradients large enough to excite the instability.

Although this explanation is consistent with experimental findings for a vertical configuration, questions still remain with regard to tilted or horizontal configurations. These cases have not been analyzed in detail but it is easy to show (mathematically) that buoyancy effects coupled with an axial gradient will destroy the unidirectional character of the flow. At present, however, neither experimental data or quantitative theoretical results are sufficient to assess this matter fully.

III. MODELING THE ELECTROPHORETIC SEPARATION IN CONTINUOUS FLOW ELECTROPHORESIS

Introduction

We turn now to the task of describing how a sample with a particular mobility distribution will be altered in its passage through a continuous flow electrophoresis chamber. To provide a first approximation we have chosen to base the model on one-dimensional approximations to the various flow and temperature fields and ignore, for the present, two-dimensional effects due to side walls at $z = \pm h$ (except insofar as they cause the electro-osmotic flow to recirculate). Consequently, the temperature and velocity fields and the particle mobility are functions of y alone. This procedure is accurate as long as $d/h \ll 1$ and regions near the side walls are ignored. The effect of the side walls requires much more extensive analysis and remains to be done.

The model for separation is based on the fact that the velocity of a particle of a given mobility can be written as a superposition of an axial velocity, u(y), and a transverse component made up of the electro osmotic flow velocity, w(y) and the particle velocity due to electrophoresis, $v_m(y)$. Thus for a particle of mobility, m, say, the velocity is

$$\hat{i}u(y) + \hat{k}[w(y) + v_m(y)] \tag{46}$$

and particles which enter with the sample at y_o, z_o will exit at $y = y_o$, $z = z_o + L[w(y) + v_m(y)]/u(y)$. If we denote the mobility distribution as $N_m(x,y,z)$, to represent the number d[illegible]ity of particles with mobility, m, then

$$u(y)\frac{\partial N_m}{\partial x} + [w(y) + v_m(y)]\frac{\partial N_m}{\partial z} = 0 \tag{47}$$

describes the fact that the particles are conserved. The number density at a point x,y,z, is, therefore,

$$N_m\{0,y,z - x[w(y) + v_m(y)]/u(y)\}$$

and the problem is simply one of "tracking".

To predict the mobility distributions at the exit from the separator we suppose that there are a number of collector tubes of area (2d)(Δ) at the outlet plane. The mobility distribution in a given collector is simply

$$\langle N_m \rangle_i = \frac{1}{\Delta}\int_{z_i}^{z_i+\Delta} \bar{N}_m(z)dz \tag{48}$$

$$\bar{N}_m(z) = \frac{\int_{-d}^{d} N_m(L,y,z)u(y)dy}{\int_{-d}^{d} u(y)dy} \tag{49}$$

A computer program was written to implement this scheme; representative results are tabulated in Table II.

Outline of the Computation Method

The computation of the mobility distribution in the collection streams proceeds as follows

Main Input Data are:

Chamber dime sions (2d and 2h)

Electrode length (ℓ)

Number of collection streams

Electric field strength

Buffer flowrate

Buffer temperature

Constants in the linear equation for buffer electrical conductivity

Constants in the linear equation for buffer thermal conductivity

Buffer conductivities for heat and electricity at the wall temperature

Coating mobility at 20°C

Mobility distribution of sample at 20°C

Location and size of sample stream.

The program then evaluates the temperature field using Eqs. (7), (13) and (15) and calculates the local values of density and viscosity using analytical formulas supplied. (Other relations can be used if necessary.) Then the local axial and electro-osmotic velocities are calculated using the appropriate equations for temperature dependent properties cited in Part I, Eqs. (23) and (30). Finally, particles on the edge of the sample are tracked to the outlet, using mobilities which reflect the local temperature, and the mobility distribution for each collector calculated. Numerical output includes

Temperature field

Axial velocity field

Electro-osmotic velocity field

Mobility distribution for each collector.

Results of two representative calculations, one with a narrow-gap chamber, the other with a wide-gap, are shown on Table II. General conditions are as shown on Table I. The sample contained two types of particles in equal amounts. Although both configurations show complete separation the wide-gap configuration separates the sample into two widely spaced collectors; the narrow-gap chamber barely separates the two fractions and if either fraction contained a distribution of mobilities there would be overlap. It was not possible to operate the wide-gap chamber model at 1-g without the recirculating flows described in Part II - so gravity had to be suppressed in the calculation.

These calculations are intended to be *illustrative* of the sorts of results that can be obtained using the models derived here. Much more extensive calculations are required to establish the differences in the separatory capabilities of various continuous flow devices.

TABLE I.

Parameters used in numerical calculations

Fluid Properties (A-1 Buffer)

Buffer Temperature	10	°C
Density	1.0	g/cm^3
Viscosity	1.33×10^{-2}	g/cm-s
Thermal Conductivity	5.82×10^{-3}	watts/cm-°C
Electrical Conductivity	6.9×10^{-4}	$(ohm\text{-}cm)^{-1}$
Coefficient of Expansion	8.62×10^{-5}	$(°C)^{-1}$
Thermal Conductivity Coefficient	2.58×10^{-3}	$(°C)^{-1}$
Electrical Conductivity Coefficient	3.12×10^{-2}	$(°C)^{-1}$

Chamber Parameters

	Narrow-Gap	Wide-Gap
Electric Field Strength, v/cm	70	70
Gravitational Constant*, cm/s^2	980	980
Gap Distance (2d), cm	0.15	0.5
Width (2h), cm	5	5
Length, cm	16	10
Volumetric Flow, cm^3/s	0.35	0.7
Average Velocity, cm/s	0.467	0.28
ΔT_r, °C	3.17	35.2
Re	2.63	5.26
N_2	8.88×10^2	1.64×10^4
N_3	2.4×10^{-1}	4.98×10^1
k_1	8.2×10^{-3}	9.1×10^{-2}
σ_1	9.9×10^{-2}	1.1

* except where noted

TABLE II

Red-Blood Cell Separation in Narrow-Gap and Wide-Gap Machines

To demonstrate the use of the separation model two runs were made at conditions shown on Table I with samples made up of equal amounts of particles ('red-blood cells') with mobilities of 2.15 μm-cm/v-s (m=1) and 4.15 μm-cm/v-s (m=2)(at 20°C).

Other conditions were:

Coating mobility 2.15 μm-cm/v-s

Sample inlet size 0.05 cm

Number of collectors 100

Locations of Separated Particles

Narrow-Gap Chamber

Chamber #	1-13	14	15	16	17	18	19	20	21-100
m = 1	0	.177	.590	.233	0	0	0	0	0
m = 2	0	0	0	0	.159	.477	.353	.021	0

Wide-Gap Chamber*

Chamber #	1-20	21	22	23	24-29	30	31	32	33-100
m = 1	0	.043	.546	.411	0	0	0	0	0
m = 2	0	0	0	0	0	.282	.610	.108	0

---

* g = 0

ACKNOWLEDGMENTS

Dr. R.S. Snyder of MSFC, Dr. G.V.F. Seaman of the University of Oregon and Dr. R.N. Griffin of General Electric have each helped us to understand the many problems involved in the electrophoresis of small particles. Kurt Hebert of Princeton University did much of the computer programming.

BIBLIOGRAPHY

Batchelor, G.K. (1972), "Sedimentation in a dilute dispersion of spheres", J. Fluid Mech. 52:245.

Carslaw, H.S. and J.C. Jaeger (1959), *Conduction of Heat in Solids*, p.404, Oxford:Clarendon Press, 510 pp., 2nd. ed.

Chandrasekhar, S. (1961), *Hydrodynamic and Hydromagnetic Stability*, Oxford: Clarendon Press, 651 pp.

Ostrach, S. (1955), "Unstable convection in vertical channels with heating from below including effects of heat sources and frictional heating", NACA Tech. Note 3458.

Ostrach, S. (1964), "Laminar flows with body forces" in *Theory of Laminar Flows*, p.528, vol. IV of *High Speed Aerodynamics*, F.K. Moore, editor, Princeton:Princeton University Press.

Ostrach, S. (1976), "The influence of convection in continuous flow electrophoresis", ESA Publication 114.

Schlichting, H. (1960), *Boundary Layer Theory*, New York:McGraw-Hill, 647 pp.

Semon, H. (1977), "Investigation of flow stability in the SPAR wide-gap electrophoretic separator chamber", General Electric Company Space Sciences Laboratory Report.

Shaw, D.J. (1969), *Electrophoresis*, New York:Academic, 144 pp.

Sparrow, R., R.J. Goldstein and V.K. Jonsson (1964), "Thermal instability in a horizontal fluid layer: effect of boundary conditions and non-linear temperature profile", J. Fluid Mech. 18:513-528.

Vest, C.M. and V.S. Arpaci (1969), "Stability of natural convection in a vertical slot", J. Fluid Mech. 39:1.

COMPUTER PROGRAMS

Four programs were written in FORTRAN IV:

ZTEMP - the two-dimensional temperature field, Eq. (12)

VELO - the two-dimensional velocity field, Eq. (19)

TRANST - the transient temperature field, Eq. (17)

TEMP - the separation model.

Listings of these are given on the following pages.

```
FORTRAN IV G LEVEL  21                MAIN               DATE = 78110        09/10/45

                  C
                  C
                  C  *******************************************************************
                  C  *
                  C  *  ZTEMP DETERMINES THE TEMPERATURE IN THE ELECTROPHORESIS CELL AS A
                  C  *  FUNCTION OF BOTH Y AND Z.  THROUGH A CALL TO THE PROCEDURE PERVUE, IT
                  C  *  THEN PLOTS A PERSPECTIVE VIEW OF THE TEMPERATURE SURFACE.  ZTEMP ACCEP
                  C  *  AS INPUT PARAMETERS VALUES OF THESE VARIABLES--
                  C  *
                  C  *     SIGMA1 - PARAMETER IN THE EXPRESSION FOR ELECTRICAL CONDUCTIVITY.
                  C  *     BI     - THE BIOT NUMBER
                  C  *     W      - THE ASPECT RATIO OF THE CHANNEL
                  C  *     NTERMS - THE NUMBER OF TERMS TO BE TAKEN IN THE SERIES FOR TEMPERA-
                  C  *              TURE
                  C  *     NYPTS - THE NUMBER OF EQUALLY SPACED CONSTANT-Y LINES FROM (AND
                  C  *              INCLUDING) Y=0 TO Y=1 ALONG WHICH TEMPERATURE IS EVALUATED.
                  C  *     NZPTS - THE NUMBER OF EQUALLY SPACED CONSTANT-Z LINES FROM (AND
                  C  *              INCLUDING) Z=0 TO Z=W ALONG WHICH TEMPERATURE IS EVALUATED.
                  C  *
                  C  *******************************************************************
                  C
                  C
      0001              DIMENSION TEMP (201,101),
                      X           YY (101),
                      X           ZZ (201)
      0002              REAL LAMBDA,LAMBD2
      0003          100 FORMAT (1H1)
      0004          110 FORMAT ('0','SIGMA1 =',1PE9.2,4X,'NO. TERMS =',I7,2X,
                      X         'ASPECT RATIO =',1PE9.2/'0','BIOT NO. =',1PE9.2,2X,
                      X         'NO. Y POINTS =',I4, 2X,'NO. Z POINTS = ',I4)
      0005          101 FORMAT ('0',9X,'Z',10X,'TEMPERATURE')
      0006          130 FORMAT (' ')
      0007          103 FORMAT ( 2(2X,1PE14.6))
      0008          150 FORMAT (3E10.3,3I5)
      0009              READ(5,150) SIGMA1,BI,W,NTERMS,NYPTS,NZPTS
      0010              PI=3.1415926
                  C
                  C
      0011              DY=1./(NYPTS-1.)
      0012              DZ=W/(NZPTS-1.)
                  C
                  C  THE OUTER LOOP INCREMENTS Y, THE NEXT INNERMOST LOOP INCREMENTS Z, AND TH
                  C  INNERMOST TWO LOOPS TAKE THE SERIES FOR TEMPERATURE OUT TO NTERMS TERMS.
                  C  THE PROGRAM STORES THE TEMPERATURE IN THE ARRAY TEMP(I,J), WITH INDICES I
                  C  J REFERRING TO THE Y-DIRECTION COORDINATE AND Z-DIRECTION COORDINATE
                  C  RESPECTIVELY.  THE ACTUAL Y AND Z COORDINATES ARE STORED IN ARRAYS YY AND
                  C
      0013              Y=-DY
      0014              DO 30 I=1,NYPTS
      0015                 Y=Y+DY
      0016                 X=PI*(1.+Y)/2.
      0017                 Z=-DZ
      0018                 DO 20 J=1,NZPTS
      0019                    Z=Z+DZ
      0020                    SUM=0.
      0021                    DO 10 K=1,NTERMS
```

ORIGINAL PAGE IS
OF POOR QUALITY

```
                N=2*K-1
                LAMBD2=N*N*PI*PI/4.-SIGMA1
                T=(1.-(-1.)**N)/N/LAMBD2
                LAMBDA=LAMBD2**0.5
                AE1=LAMBDA*(Z-W)
                AE2=-LAMBDA*(Z+W)
                AE3=-2.*LAMBDA*W
                IF (AE1+50.) 1,1,2
      1         E1=0.
                GO TO 3
      2         E1=EXP(AE1)
      3         IF (AE2+50.) 4,4,5
      4         E2=0.
                GO TO 6
      5         E2=EXP(AE2)
      6         IF (AE3+50.) 7,7,8
      7         E3=0.
                GO TO 9
      8         E3=EXP(AE3)
      9         CONTINUE
                T1=(E1+E2)/(LAMBDA*(1.-E3)-BI*(1.+E3))
                B=T+T*BI*T1
     10         SUM=SUM+B*SIN(N*X)
             TEMP(J,I)=2.*SUM/PI
     20      ZZ(J)=Z
     30   YY(I)=Y
          TEMP1=TEMP(1,1)
C
C     PLOT THE TEMPERATURE FIELD AS A SURFACE VIEWED IN PERSPECTIVE.
C
          K=2*NYPTS
          DO 60 I=1,NYPTS
             K=K-1
          L=2*NZPTS
             DO 50 J=1,NZPTS
                L=L-1
     50         TEMP(L,K)=TEMP(NZPTS+1-J,NYPTS+1-I)
     60         CONTINUE
          NYM=NYPTS-1
          NZM=NZPTS-1
          K=2*NYPTS
          DO 62 I=1,NYPTS
             K=K-1
             DO 62 J=1,NZM
     62      TEMP(NZPTS-J,K)=TEMP(NZPTS+J,K)
          NY=2*NYPTS-1
          NZ=2*NZPTS-1
          DO 65 J=1,NZ
             DO 65 I=1,NYM
     65      TEMP(J,NYPTS-I)=TEMP(J,NYPTS+I)
          Z=-DZ-W
          DO 70 J=1,NZ
             Z=Z+DZ
     70      ZZ(J)=Z
          Y=-DY-1.
          DO 80 I=1,NY
```

FORTRAN IV G LEVEL 21 MAIN DATE = 78110 09/10/45

```
0075            Y=Y+DY
0076      80    YY(I)=Y
0077          JT=TEMP1*10.+1.
0078          NCONTR=JT*2
0079          TMAX=JT/10.
       C
       C  PRINT THE FIELD FOR Y=0.
       C
0080          WRITE (6,100)
0081          WRITE (6,110)SIGMA1,NTERMS,W,BI,NYPTS,NZPTS
0082          WRITE (6,101)
0083          WRITE (6,120)
0084          DO 40 J=1,NZ
0085      40    WRITE(6,103) ZZ(J),TEMP(J,NYPTS)
       C
       C      PRINT THE FIELD FOR Z=0.
       C
0086          WRITE (6,102)
0087     102 FORMAT ('0',9X,'Y',10X,'TEMPERATURE')
0088          DO 41 I=1,NY
0089      41    WRITE (6,103) YY(I),TEMP(NZPTS,I)
0090          CALL PLAVUE (11,ZZ,YY,IEMP,W+0.5,4.,TMAX+1.5,201,101,NZ,NY,0,
             X NCONTR,0,-.1,TMAX,0,0,0,9.,4.,-1,17,'TEMPERATURE FIELD')
0091          STOP
0092          END
```

ORIGINAL PAGE IS
OF POOR QUALITY

```
                C
                C
                C
                C  ***********************************************************************
                C  *
                C  *  VELO DETERMINES THE DOWNWARD VELOCITY IN THE ELECTROPHORESIS CELL AS A
                C  *  FUNCTION OF BOTH Y AND Z. THROUGH A CALL TO THE PROCEDURE PERVUE, IT
                C  *  THEN PLOTS A PERSPECTIVE VIEW OF THE VELOCITY SURFACE.
                C  *
                C  *     SIGMA1    -PARAMETER IN THE EXPRESSION FOR THE ELECTRICAL
                C  *                CONDUCTIVITY
                C  *     BI        -THE BIOT NUMBER
                C  *     W         -THE ASPECT RATIO OF THE CHANNEL
                C  *     NTERMS    -THE NUMBER OF TERMS TO BE TAKEN IN THE SERIES FOR THE
                C  *                VELOCITY
                C  *     NYPTS     -THE NUMBER OF EQUALLY SPACED CONSTANT-Y LINES ROC (AND
                C  *                INCLUDING) Y=0 TO Y=1 ALONG WHICH THE VELOCITY IS
                C  *                EVALUATED
                C  *     NZPTS     -THE NUMBER OF EQUALLY SPACED CONSTANT-Z LINES EOD (AND
                C  *                INCLUDING) Z=0 TO Z=W ALONG WHICH VELOCITY IS EVALUATED
                C  *
                C  ***********************************************************************
                C
                C
0001                DIMENSION U(201,101),YY(101),ZZ(201)
0002                REAL LAMBDA,LAMBD2,N2,N3
0003            100 FORMAT (1H1)
0004            110 FORMAT ('0', 2X,'SIGMA1 =',E10.3,2X,'BIOT NO. =',E10.3,2X,
                   X        'ASPECT RATIO =',E10.3,2X,'N2 =',E10.3,2X,'N3 =',E10.3)
0005            111 FORMAT ('0',2X,'NTERMS =',I5,2X,'NYPTS =',I5,2X,'NZPTS =',I5)
0006            120 FORMAT ('0',9X,'Z',11X,'X VELOCITY')
0007            130 FORMAT (' ')
0008            140 FORMAT (2(2X,1PE14.6))
0009            150 FORMAT (5E10.3,3I5)
0010            160 FORMAT ('0',9X,'Y',11X,'X VELOCITY')
0011                READ (5,150,END=999) SIGMA1,BI,W,N2,N3,NTERMS,NYPTS,NZPTS
0012                WRITE (6,100)
0013                WRITE (6,110) SIGMA1,BI,W,N2,N3
0014                WRITE (6,111) NTERMS,NYPTS,NZPTS
0015                UMIN=0.
0016                UMAX=0.
0017                PI=3.1415926
0018                PI2=PI*PI
0019                PI24=PI2/4.
0020                PI4=PI/4.
0021                PIW=PI*W
0022                WPI2=PI*W/2.
0023                TPI=2./PI
0024                SUM1=0.
0025                SUM2=0.
0026                SUM3=0.
0027                K=-1
                C
                C  DETERMINE THE CONSTANT, K, FROM THE INTEGRATED VELOCITY.
                C
0028                DO 5 N=1,NTERMS
```

```
      K=K+2
      LAMBD2=K*K*PI24-SIGMA1
      LAMBDA=LAMBD2**0.5
      FN2=K*K
      FN4=FN2*FN2
      B1=1BI/K
      FTANH1=TANH(K*BPI2)
      FTANH2=TANH(LAMBDA*W)
      S1=(B1*FTANH1-W)/FN4
      S2=S1/LAMBD2
      S3=(( B1*FTANH1-FTANH2/LAMBDA)/(LAMBDA*FTANH2-BI))/FN2/LAMBD2
      SUM1=SUM1+S1
      SUM2=SUM2+S2
      SUM3=SUM3+S3
    5 CONTINUE
      A1=SUM1*32./W/(PI**4)
      A2=SUM2*32./W/(PI**4)
      A3=SUM3*8./SIGMA1/PI/PI/W
      FK=(1.+N2*A1-N3*A2-N3*BI*A3)/A1
      WRITE (6,112) FK
  112 FORMAT (' ',2X,E10.3)
C
C  EVALUATE VELOCITY AT EACH (Y,Z) POINT TAKEN.
C
      DY=1./(NYPTS-1.)
      DZ=W/(NZPTS-1.)
      Y=-DY
      FK1=FK-N2
      F1=8./PI2
      F2=2.*N3*BI/SIGMA1
      DO 30 I=1,NYPTS
         Y=Y+DY
         Z=BI*(1.+Y)/2.
         Z=-DZ
         DO 20 J=1,NZPTS
            Z=Z+DZ
            SUM=0.
            K=-1
            DO 10 N=1,NTERMS
               K=K+2
               LAMBD2=K*K*PI24-SIGMA1
               LAMBDA=LAMBD2**0.5
               FK3=K**3
               FTANH=TANH(LAMBDA*W)
               C1=F1*(FK1+N3/LAMBD2)/FK3
               C3=F2/K/LAMBD2
               C2=C3/(LAMBDA*FTANH-BI)
               ARG1=K*(Z-W)/TPI
               ARG2=-K*(Z+W)/TPI
               ARG3=-K*PIW
               ARG4=LAMBDA*(Z-W)
               ARG5=-LAMBDA*(Z+W)
               ARG6=-2.*LAMBDA*W
               IF (ARG1.LE.-100.) E1=0.
               IF (ARG1.GT.-100.) E1=EXP(ARG1)
               IF (ARG2.LE.-100.) E2=0.
```

```
                  IF (ARG2.GT.-100.) E2=EXP(ARG2)
                  IF (ARG3.LE.-100.) E3=0.
                  IF (ARG3.GT.-100.) E3=EXP(ARG3)
                  IF (ARG4.LE.-100.) E4=0.
                  IF (ARG4.GT.-100.) E4=EXP(ARG4)
                  IF (ARG5.LE.-100.) E5=0.
                  IF (ARG5.GT.-100.) E5=EXP(ARG5)
                  IF (ARG6.LE.-100.) E6=0.
                  IF (ARG6.GT.-100.) E6=EXP(ARG6)
                  E=(E1+E2)/(1.+E3)
                  A1=C1*E
                  A2=C2*E
                  A3=-C3*(E4+E5)/(LAMBDA*(1.-E6)-BI*(1.+E6))
                  A4=-C1
                  SUM=SUM+(A1+A2+A3+A4)*SIN(K*X)
   10             CONTINUE
               U(J,I)=-2.*SUM/PI
         IF (U(J,I).LE.UMIN) UMIN=U(J,I)
         IF (U(J,I).GT.UMAX) UMAX=U(J,I)
   20          ZZ(J)=Z
   30     YY(I)=Y
C
C     PLOT THE VELOCITY FIELD AS A SURFACE VIEWED IN PERSPECTIVE.
C
         K=2*NYPTS
         DO 60 I=1,NYPTS
         K=K-1
         L=2*NZPTS
            DO 50 J=1,NZPTS
               L=L-1
   50          U(L,K)=U(NZPTS+1-J,NYPTS+1-I)
   60    CONTINUE
         NYM=NYPTS-1
         NZM=NZPTS-1
         K=2*NYPTS
         DO 62 I=1,NYPTS
            K=K-1
          DO 62 J=1,NZM
   62     U(NZPTS-J,K)=U(NZPTS+J,K)
         NZ=2*NZPTS-1
         NY=2*NYPTS-1
         DO 65 J=1,NZ
            DO 65 I=1,NYM
   65       U(J,NYPTS-I)=U(J,NYPTS+I)
         U(1,1)=0.
         U(NZ,1)=0.
         U(1,NY)=0.
         U(NZ,NY)=0.
         Z=-DZ-W
         DO 70 J=1,NZ
            Z=Z+DZ
   70       ZZ(J)=Z
         Y=-DY-1.
         DO 80 I=1,NY
            Y=Y+DY
   80       YY(I)=Y
```

```
FORTRAN IV G LEVEL  21                  MAIN                DATE = 76110          09/14/24

 0135              WRITE (6,120)
 0136              WRITE (6,130)
 0137              DO 40 I=1,NZ
 0138           40 WRITE (6,140) ZZ(I),U(I,NYPTS)
 0139              WRITE (6,160)
 0140              WRITE (6,130)
 0141              DO 90 I=1,NY
 0142           90 WRITE (6,140) YY(I),U(NZPTS,I)
 0143              UMIN=1.1*UMIN
 0144              UMAX=1.1*UMAX
 0145              CALL PERVUE(11,ZZ,YY,U,N+.5,3.,3.,201,101,NZ,NY,0,10,0,UMIN,UMAX,
                  X             0,0,0,9.,9.,-1,14,'VELOCITY FIELD')
 0146          999 STOP
 0147              END
```

```
FORTRAN IV G LEVEL  21                MAIN              DATE = 76104          15/06/50

      C
      C
      C  ***********************************************************************
      C  *
      C  *  TRANSNT DETERMINES THE AVERAGE TEMPERATURE AND CENTER TEMPERATURE OF
      C  *  THE ELECTROPHORESIS CHANNEL AS FUNCTIONS OF TIME.  THE REQUIRED INPUT
      C  *  DATA IS LISTED IN THE OUTPUT OF THE PROGRAM.  ALL THE INPUT VARIABLES
      C  *  SELF-EXPLANATORY EXCEPT THE FOLLOWING-
      C  *
      C  *    NUMTAU - THE NUMBER OF TIMES AT WHICH TEMPERATURE IS EVALUATED.
      C  *    CTAU   - THE DIMENSIONLESS TIME TO WHICH TEMPERATURE IS EVALUATED
      C  *    NTERMS - THE NUMBER OF TERMS TAKEN FOR TAU = 0 IN THE SERIES FOR
      C  *             TEMPERATURE.  FOR TAU GREATER THAN ZERO, THE NUMBER OF TERMS
      C  *             TAKEN IS CONTROLLED BY NUNDER.
      C  *
      C  ***********************************************************************
      C
      C
            DIMENSION CTEMP(1001)
            DIMENSION AVTEMP(1001)
            DIMENSION T(1001)
            DIMENSION TIME(1001)
            DIMENSION NUNDER(1001)
        101 FORMAT (7E10.3)
        102 FORMAT (2I5,2E10.3)
        103 FORMAT ( 1H1)
        104 FORMAT ('0','THERMAL CONDUCTIVITY -',1PE10.2,1X,'WATTS/CM-C',2X,
           X        'DENSITY -',1PE10.2,1X,'G/CC',2X,'SPECIFIC HEAT -',1PE10.2
           X        ,1X,'CAL/C-G'/'0','ELECTRIC CONDUCTIVITY -',1PE10.2,1X,
           X        '/OHM-CM',2X,'FIELD STRENGTH -',1PE10.2,1X,'V/CM'/'0',
           X        'HALF DEPTH -',1PE10.3,1X,'CM',2X,'BUFFER TEMP. -',1PE10.3
           X        ,1X,
           X        'C')
        105 FORMAT ('0','NUMTAU =',I7,2X,'NTERMS =',I7,2X,'SIGMA1 =',1PE10.2,
           X        2X,'CTAU =',1PE10.2)
        106 FORMAT ('0',6X,'SECONDS',9X,'AVTEMP-C',8X,'CTEMP-C')
        107 FORMAT (' ')
        108 FORMAT (3(2X,1PE14.6))
            READ (5,101) THCOND,DENSTY,SPHT,ELCOND,E0,DEPTH,TBUFF
            READ (5,102) NUMTAU,NTERMS,SIGMA1,CTAU
            WRITE (6,103)
            WRITE (6,104) THCOND,DENSTY,SPHT,ELCOND,E0,DEPTH,TBUFF
            WRITE (6,105) NUMTAU,NTERMS,SIGMA1,CTAU
            FN1=SIGMA1**0.5
            CSN=COS(FN1)
            PI=3.1415926
            A=(1./CSN-1.)/SIGMA1
            B=TAN(FN1)/FN1/SIGMA1-1./SIGMA1
            DTAU=CTAU/(NUMTAU-1)
      C
      C  COMPUTE THE TIME AND TEMPERATURE SCALES FROM THE DIMENSIONED INPUT VARIABL
      C
            TMPSCL=ELCOND*E0*E0*DEPTH*DEPTH/THCOND
            TIMSCL=4*DEPTH*DEPTH*DENSTY*SPHT/THCOND*4.184
      C
      C  NUNDER SPECIFIES THE NUMBER OF TERMS TAKEN IN THE SERIES FOR TEMPERATURE,
```

FORTRAN IV G LEVEL 21 MAIN DATE = 76104 15/00/59

```
      C  FOR TAU GREATER THAN ZERO.  IF MORE THAN NUMBER TERMS ARE TAKEN, EXPONENTIAL
      C  UNDERFLOW MAY OCCUR.
      C
            NO=NUMTAU-1
            DO 4 J=1,NO
               I=J+1
               TAU=(I-1)*DTAU
      4        NUMBER(I)=.5*((16./TAU)**.5-1.)
            NUMBER(1)=NTERMS
      C
            TAU=-DTAU
            DO 7 JTAU=1,NUMTAU
               TAU=TAU+DTAU
               AVSUM=0.
               CSUM=0.
               M1=1+NUMBER(JTAU)
               DO 6 M=1,M1
                  N=M-1
                  TN=2*N+1
                  TN2=TN*TN
                  EX=EXP((-TN2*PI*PI+4.*SIGMA1)*TAU)
                  D=(4.*SIGMA1-TN2*PI*PI)
                  AVSUM=AVSUM+EX/TN2/D
      6           CSUM=CSUM+EX*(-1.)**N/D/TN
               AVTEMP(JTAU)=B+32./PI/PI*AVSUM
               AVTEMP(JTAU)=TBUFF+TMPSCL*AVTEMP(JTAU)
               CTEMP(JTAU)=A+16./PI*CSUM
      7        CTEMP(JTAU)=TBUFF+TMPSCL*CTEMP(JTAU)
      C
      C  PRINT AND PLOT (THROUGH DRIPS) THE TEMPERATURE AS A FUNCTION OF TIME.
      C
            WRITE (6,106)
            WRITE (6,107)
            TAU=-DTAU
            DO 5 K=1,NUMTAU
               TAU=TAU+DTAU
               TA=TAU*TIMSCL
               TIME(K)=TA
      5        WRITE(6,108) TIME(K),AVTEMP(K),CTEMP(K)
            SX=7.5
            CALL DRIPS1(TIME,CTEMP,NUMTAU,01,SX,
           X            '(''RELAXATION'')',0,'(''SECONDS'')',0,
           X            '(''DEGREES CENTIGRADE'')',0)
            CALL DRIPS2(TIME,AVTEMP,NUMTAU,01)
            CALL DRIPS3(3.,5.,2,'(''AVERAGE'')',0)
            CALL DRIPS3(3.,7.5,2,'(''CENTER'')',0)
            STOP
            END
```

ORIGINAL PAGE IS OF POOR QUALITY

```
FORTRAN IV G LEVEL  21                  MAIN                 DATE = 78104          15/01/24

                 C
                 C  *********************************************************************
                 C  *  TEMP EVALUATES AS FUNCTIONS OF Y THE TEMPERATURE PROFILE AND X- AND
                 C  *  Z- DIRECTION VELOCITY PROFILES FOR AN ELECTROPHORESIS CELL WITH HEAT
                 C  *  CONDUCTION IN THE Y-DIRECTION. IT ALSO MODELS PARTICLE SEPARATION FOR
                 C  *  AN INPUT STREAM OF GIVEN SIZE, LOCATION AND MOBILITY DISTRIBUTION.
                 C  *  THERE ARE TWO SUBROUTINES-  SIMPS, WHICH PERFORMS INTEGRATION BY
                 C  *  SIMPSON'S RULE, AND TEMP, WHICH COMPUTES THE TEMPERATURE FIELD.
                 C  *  AMONG THE INPUT VARIABLES ARE--
                 C  *
                 C  *
                 C  *    NVEL        -NUMBER OF POINTS AT WHICH THE VELOCITY IS EVALUATED
                 C  *                 NVEL MUST BE ODD
                 C  *    NCOL        -THE NUMBER OF COLLECTOR UNITS
                 C  *    NPCOL       -THE NUMBER OF POINTS IN EACH COLLECTOR
                 C  *                -NPCOL MUST BE ODD
                 C  *    NM          -THE NUMBER OF POINTS TAKEN IN THE MOBILITY DIST.
                 C  *    FMOBL       -ARRAY REPRESENTING MOBILITIES
                 C  *    NSUM        -NUMBER OF TERMS TAKEN IN THE INFINITE SERIES FOR THE
                 C  *                 FIRST ORDER TEMPERATURE FIELD
                 C  *    FMOBL       -ARRAY REPRESENTING THE MOBILITIES
                 C  *    FNMOBL       -ARRAY REPRESENTING THE MOBILITY CONCENTRATIONS.
                 C  *********************************************************************
                 C
                 C
                 C
0001                 DIMENSION T(2001),TMU(2001),FMU(1001),FMUI(1001),B1(1001),U1(501)
                X             ,U2(501),B(501),A(501),YY(501),U(501),ZMIN(501),
                X             ZMAX(1001),ZF(1001),ZF2(1001),AA(100 ),BM(1001),
                X             FNEAR(1001),
                X             FMOBL( 50),FNMOBL( 50),CMOBL(1001)
0002                 REAL MUO MU1
                 C
0003            101 FORMAT (5I5)
0004            102 FORMAT (4E10.3)
0005            103 FORMAT (2E10.3)
0006            104 FORMAT (3E10.3)
0007            105 FORMAT (4E10.3)
0008            106 FORMAT (2E10.3)
0009            110 FORMAT ('1','INTEGER INPUT VARIABLES')
0010            111 FORMAT (' ','NVEL -',I5,2X,'NCOL -',I5,2X,'NPCOL -',I5,2X,
                X            'NM -',I5,2X,'NSUM -',I5)
0011            112 FORMAT ('0',' '/'0','BUFFER PROPERTIES (CONSTANT)')
0012            113 FORMAT (' ','VISCOSITY -',1PE10.2,1X,'GM/CM-S',2X,'DENSITY -',
                X           1PE10.2,1X,'GM/CC',2X,'THERMAL CONDUCTIVITY -',1PE10.2,
                X           1X,'WATTS/CM-C'/' ELECTRIC CONDUCTIVITY -',1PE10.2,
                X           1X,'/OHM-CM')
0013            114 FORMAT ('0',' '/'0',
                X           'BUFFER PROPERTITIES (TEMPERATURE VARYING, DIMENSIONLESS)')
0014            115 FORMAT ('0','THERM. COND.',6X,'ELECT. COND.')
0015            116 FORMAT (' ','FKP1 =',1PE10.3,2X,'FS1P =',1PE10.3)
0016            117 FORMAT (' ','FKP2 =',1PE10.3,2X,'FS2P =',1PE10.3)
0017            118 FORMAT ('0',' '/'0','CHAMBER DIMENSIONS')
0018            119 FORMAT (' ','WIDTH -',1PE10.2,1X,'CM',2X,'LENGTH -',1PE10.2,1X,
                X           'CM',2X,'DEPTH -',1PE10.2,1X,'CM')
0019            120 FORMAT ('1',2X,'MOBILITY (MICRONS-CM/VOLT-S)',2X,'COLLECTOR',2X,
```

```
                    X         'MOBILITY DENSITY')
0020            121 FORMAT (' ',1PE10.2,20X,1PE10.2)
0021            122 FORMAT ('0',' '/'0','ELECTRIC FIELD STRENGTH -',E10.2,1X,'V/CM',2X
                    X        ,'BUFFER TEMPERATURE -',E10.2,1X,'C',2X,'BUFFER FLOW RATE -
                    X        ',E10.2,1X,'CC/S',/' ','COATING MOBILITY -',E10.2,1X,
                    X        'MICRONS-CM/V-S')
0022            123 FORMAT ('1',2X,'MOBILITY (MICRONS-CM/VOLT-S)',2X,'MOBILITY DENSITY
                    X')
0023            124 FORMAT ('0',2X,'Y (CM)',1X,'TEMPERATURE (C)',6X,'U (CM/S)',6X,
                    X        'W (CM/S)')
0024            125 FORMAT (' ')
0025            126 FORMAT (' ',F5.3,3(3X,1PE14.6))
0026            127 FORMAT (' ',9X,E14.4,11X,I5,3X,E14.4)
0027            128 FORMAT ('0','PARTICLES OF MOBILITY',1PE10.2,2X,
                    X        'LOST FROM INITIAL POSITION Y =',E14.5)
0028            129 FORMAT (' ','Y1 =',E14.5,2X,'Z1 =',E14.5,2X,'R =',E14.5)
0029            130 FORMAT (I5)
0030            131 FORMAT (1E10.3)
0031            132 FORMAT (' ','GRAVITATIONAL FIELD STRENGTH =',E14.5,'CM/S**2')
0032            133 FORMAT ('0', 'SAMPLE INLET LOCATION AND SIZE'/' ','COORDINATES   Y
                    X        -',I4,2X,E10.3,2X,'Z-',I4,2X,E10.3,2X,'SAMPLE RADIUS  '
                    X        ,2X,E10.3)
0033            134 FORMAT ('0',2X,'Y',6X,'TEMPERATURE',10X,'U',15X,'W')
0034            135 FORMAT ('1')
                C
0035                READ (5,101) NVEL,NCOL,NPCCL,NS,NSUB
0036                READ (5,102) FSP1,FSP2,FKP1,FKP2
0037                READ (5,103) ELCOND,THCOND
0038                READ (5,104) WIDTH,DEPTH,XLONG
0039                READ (5,104) Y1,Z1,R
0040                READ (5,105) E0,TBUFF,CTMOBL,QBUFF
0041                READ (5,131) GRAV
0042                READ (5,106) (FMOBL(I),FNMOBL(I),I=1,N4)
                C
                C
                C EVALUATE TEMPERATURE FIELD AS ARRAY T- GIVES TEMPERATURE AT NTEMP POINTS
                C  FROM Y=0 TO Y=1.
                C
0043                NDE=2*NVEL-1
0044                NTEMP=2*NDE-1
0045                TSCALE=ELCOND*E0*E0*DEPTH*DEPTH/THCOND/4.
0046                T1=TBUFF
0047                T2=T1**2
0048                T3=T1**3
0049                DENSIY=0.998203/(1.-(0.6042E-05)*T1+(8.5055E-06)*T2-(6.79E-08)*T3)
0050                CALL TEMP(NTEMP,NSUP,FSP1,FKP1,T)
                C
                C  EVALUATE DENSITY AT EACH TEMPERATURE POINT- ARRAY RHO
                C
0051                CRHO=0.998203/DENSIY
0052                DO 2 I=1,NTEMP
0053                FT=TBUFF+TSCALE*T(I)
0054                FT2=FT**2
0055                FT3=FT**3
0056                RHO(I)=CRHO/(1.-(0.06042E-5)*FT+(8.5055E-6)*FT2-(6.79E-8)*FT3)
0057              2 CONTINUE
```

ORIGINAL PAGE IS
OF POOR QUALITY

```
FORTRAN IV G LEVEL  21                MAIN              DATE = 78104           15/31/54

      C
      C  EVALUATE VISCOSITY AT EVERY OTHER TEMPERATURE POINT- ARRAY FMU
      C
            J=-1
            ARG =TBUFF-20.
            ARG=3.00067/(1.+0.0082*ARG)
            ARG=-7.6039+ARG
            MU0=EXP(ARG)
            MU1=0.008937
            CTMOEL=CTMCBL*MU1/MU0
            VISC=MU0
            DO 3 I=1,NDP
               J=J+2
            ARG=TSCALE*T(J)+TBUFF-20.
            ARG=3.00067/(1.+0.0082*ARG)
            ARG=-7.6039+ARG
            FMU(I)=EXP(ARG)/MU0
          3 CONTINUE
            WRITE (6,110)
            WRITE (6,111) NVEL,NCCL,NPCCL,N4,NSU4
            WRITE (6,112)
            WRITE (6,113) VISC,DENSTY,THCOND,ZICCND
            WRITE (6,114)
            WRITE (6,115)
            WRITE (6,116) FNP1,FSP1
            WRITE (6,117) FNP2,FSP2
            WRITE (6,118)
            WRITE (6,119) WIDTH,XLONG,DEPTH
            WRITE (6,122) DO,TBUFF,CBUFF,CTMCBL
            WRITE (6,129) Y1,Z1,R
            WRITE (6,132) GRAV
            WRITE (6,123)
            WRITE (6,121) (FNCEL(I),FNMOEL(I),I=1,NM)
      C
      C
      C  COMPUTE DENSITY INTEGRAL AS ARRAY FRHOI REPRESENTING DENSITY INTEGRATED F
      C  Y=0 TO EVERY OTHER DENSITY-TEMPERATURE POINT
      C
            DY=1./(NTEMP-1.)
            FRHOI(1)=0.
            N1=1
            N2=3
            DO 4 I=2,NDP
               A=DY*(RHO(N1)+4.*RHO(N1+1)+RHO(N2))/3.
               N1=N2
               N2=N2+2
               FRHOI(I)=A+FRHOI(I-1)
          4 CONTINUE
      C
      C  COMPUTE Y/FMU INTEGRAL AS ARRAY REPRESENTING Y/FMU INTEGRATED FROM Y=0 TO
      C  EVERY OTHER VISCOSITY POINT (I.E., EVERY FOURTH DENSITY-TEMPERATURE POINT
      C  FIRST EVALUATE Y/FMU AS ARRAY S1.
      C
            DY=1./(NDP-1.)
            S1(1)=0.
            DO 5 I=2,NDP
```

```
FORTRAN IV G LEVEL  21                 MAIN              DATE = 78104          15/31/34

0101              Y=DY*(I-1)
0102              S1(I)=Y/FNU(I)
0103         5 CONTINUE
0104            U1(1)=C.
0105            N1=1
0106            N2=3
0107            DO 6 I=2,NVEL
0108              A=DY*(S1(N1)+4.*S1(N1+1)+S1(N2))/3.
0109              N1=N2
0110              N2=N1+2
0111              U1(I)=A+U1(I-1)
0112         6 CONTINUE
          C
          C  EVALUATE FRHOI/FNU AS ARRAY U2 REPRESENTING FRHOI/FNU INTEGRATED FROM Y=0
          C  EVERY OTHER VISCOSITY POINT.  FIRST EVALUATE FRHOI/FNU AS ARRAY S1.
          C
0113            S1(1)=C.
0114            DO 7 I=2,NDF
0115              S1(I)=FRHOI(I)/FNU(I)
0116         7 CONTINUE
0117            U2(1)=C.
0118            N1=1
0119            N2=N1+2
0120            DO 8 I=2,NVEL
0121              A=DY*(S1(N1)+4.*S1(N1+1)+S1(N2))/3.
0122              N1=N2
0123              N2=N1+2
0124              U2(I)=A+U2(I-1)
0125         8 CONTINUE
          C
          C  CHANGE U1 AND U2 FROM INTEGRALS TAKEN FROM ZERO TO Y TO THEIR FORM IN THE
          C  VELOCITY EXPRESSION- TAKEN FROM Y TO 1.
          C
0126            DO 11 I=1,NVEL
0127              U1(I)=U1(NVEL)-U1(I)
0128        11    U2(I)=U2(NVEL)-U2(I)
          C
          C  EVALUATE THE CONSTANT FK BY INTEGRATING -FK*U1 + K2*U2 FROM Y=0 TO Y=1
          C  AND SETTING RESULT EQUAL TO ONE.
          C
0129            DY=1./(NVEL-1.)
0130            N1=1
0131            CALL SIMPS(DY,U1,N1,NVEL,A1)
0132            CALL SIMPS(DY,U2,N1,NVEL,A2)
0133            FNU=VISC/DENSTY
0134            USCALE=QBUFF/WIDTH/DEPTH
0135            FK2=GRAV*DEPTH*DEPTH/FNU/USCALE/4.0
0136            FK=(-1.+FK2*A2)/A1
          C
          C  EVALUATE THE    AL VELOCITY
          C
0137            USUM=0.
0138            DO 9 I=1,NVEL
0139              U(I)=-FK*U1(I)+FK2*U2(I)
0140         9    USUM=USUM+U(I)
          C
```

ORIGINAL PAGE IS
OF POOR QUALITY

```
FORTRAN IV G LEVEL  21                  MAIN               DATE = 78104          [illegible]

C  COMPUTE THE ELECTROOSMOTIC (Z-DIRECTION) VELOCITY.  THIS HAS THE FORM OF [illegible]
C  SO MERELY USE INTEGRATED U1 TO DETERMINE CONSTANT, AND THEN SUBTRACT 1.
C
       WSCALE=ETMOBI*EC*.0001
       PK2=-1./A1
       WSUM=0.
       J=-1
       DO 12 I=1,NVEL
       J=J+2
       CMOBI(I)=0.0001*MU1/(MUO*FMO(J))
          W(I)=-PK2*U1(I)-1.
   12     WSUM=WSUM+W(I)
C
C  PRINT TEMPERATURE AND U- AND W- VELOCITY FIELDS AT VALUES OF Y CORRESPONDING
C  TO THE VELOCITY POINTS.
C
       DY=1./(NVEL-1)
       WRITE (6,135)
       WRITE (6,134)
       WRITE (6,125)
       DO 30 I=1,NVEL
       Y=DY*(I-1)
       J=1+(I-1)*4
   30  WRITE (6,126) Y,T(J),U(I),W(I)
       DY=DY*DEPTH/2.
       WRITE (6,135)
       WRITE (6,124)
       WRITE (6,125)
       DO 10 I=1,NVEL
          Y=DY*(I-1)
          J=1+(I-1)*4
          U(I)=U(I)*USCALE
          W(I)=W(I)*WSCALE
          T(J)=T(J)*TSCALE+TBUFF
   10     WRITE (6,126) Y,T(J),U(I),W(I)
C
C
       J=2*NVEL
       DO 14 I=1,NVEL
          J=J-1
       CMOBI(J)=CMOBI(NVEL+1-I)
          U(J)=U(NVEL+1-I)
   14     W(J)=W(NVEL+1-I)
       NVELM=NVEL-1
       DO 15 I=1,NVELM
       CMOBI(NVEL-I)=CMOBI(NVEL+I)
          U(NVEL-I)=U(NVEL+I)
   15     W(NVEL-I)=W(NVEL+I)
       NV=2*NVEL-1
       YZ=DEPTH/2.
       Y=-YZ-DY
       DO 16 I=1,NV
          Y=Y+DY
       YY(I)=Y
   16  CONTINUE
C
```

```
          C  SET THE Z-COORDINATE ARRAY AND THE Z-DIRECTION STEP SIZE.
          C
0187            ZCOL=WIDTH/NCOL
0188            DZ=ZCOL/(NPCOL-1)
0189            NZ=(NPCOL-1)*NCOL+1
0190            ZW=WIDTH/2.
0191            NYPTS=NVEL
0192            NZPTS=(NZ-1)/2+1
0193            Z=-ZW-DZ
0194            DO 190 I=1,NZ
0195            Z=Z+DZ
0196        190 ZZ(I)=Z
          C
          C  ROUND THE CENTER AND RADIUS OF THE SAMPLE STREAM TO THE NEAREST MULTIPLES
          C  OF DY.
          C
0197            IY1=(Y1/DY+.5)+NYPTS
0198            IZ1=(Z1/DZ+.5)+NZPTS
0199            Y1=YY(IY1)
0200            Z1=ZZ(IZ1)
0201            NR=R/DY+.5
0202            R=NR*DY
0203            WRITE (6,133) IY1,Y1,IZ1,Z1,R
          C
          C  FOR EACH MOBILITY TAKEN IN THE SAMPLE DISTRIBUTION, DETERMINE THE EXIT
          C  LOCATIONS OF PARTICLES ON THE EDGE OF THE SAMPLE STREAM.
          C
0204            M=IY1-R/DY-1
0205            NYM=2.*(R/DY)+1.
0206            DO 200 J=1,NYM
0207               I=J+M
0208               P=(ABS(R*R-(YY(I)-Y1)*(YY(I)-Y1)))**.5
0209               ZMIN(J)=Z1-P
0210        200 CONTINUE
0211            WRITE (6,120)
0212            DO 270 J=1,NM
0213               DO 270 K=1,NYM
0214                  L=K+M
0215                  ZF(K)=ZMIN(K)+XLONG*(W(L)+EO*FMCOL(J)*CACOS(L))/U(L)
0216                  IF(YY(L).GT.YD.OR.YY(L).LE.-YD)
               X         ZF(K)=999.
0217                  P=(ABS(R*R-(YY(L)-Y1)*(YY(L)-Y1)))**.5
0218                     ZF2(K)=ZF(K)+2.*P
0219                     IF (ZF(K).LE.-ZW)
               X            WRITE (6,128) FMCOL(J),YY(L)
0220        270          IF (ZF2(K).GE.ZW)
               X            WRITE (6,128) FMCOL(J),YY(L)
          C
          C  FIND THE Y-AVERAGED MOBILITY DISTRIBUTIONS AT EACH Z POINT.
          C
0221            DO 230 I=1,NZ
0222                  DO 210 K=1,NYM
0223                     L=K+M
0224                     IF (ZZ(I).GE.ZF(K).AND.ZZ(I).LE.ZF2(K))
               X            AM(K)= FNMCOL(J)*U(L)
0225        210          IF (ZZ(I).LT.ZF(K).OR.ZZ(I).GT.ZF2(K))
```

```
FORTRAN IV G LEVEL  21                 MAIN              DATE = 76104          15/01/34
                      X           AM(K)=0.
 0226                          CALL SIMPS(DY,AM,1,NYM,D)
 0227                          FNBAR(I)=D/USCALE/DEPTH
 0228               230    CONTINUE
                  C
                  C  FIND THE AVERAGE MOBILITY DISTRIBUTION IN EACH SAMPLE COLLECTOR.
                  C
 0229                   NDIV=NPCCL-1
 0230                   DO 260 J=1,NCCL
 0231                      JINIT=(J-1)*NDIV
 0232                         DO 240 K=1,NPCCL
 0233                            L=K+JINIT
 0234               240          BM(K)=FNBAR(L)
 0235                      CALL SIMPS(DZ,BM,1,NPCCL,C)
 0236                      C=C/ZCCL
                  C
                  C  PRINT THE COLLECTOR MOBILITY DISTRIBUTIONS.
                  C
 0237                   WRITE (6,127) FMOBL(J),J,C
 0238              260     CONTINUE
 0239              300     CONTINUE
 0240               99 STOP
 0241                   END
```

```
FORTRAN IV G LEVEL  21                TEMP                DATE = 78104          15/01/34

      SUBROUTINE TEMP(NI,NS,FS,FKP,T)
C
C THE TEMP SUBROUTINE EVALUATES THE TEMPERATURE FIELD T = TZERO + FKP*TONE
C TZERO IS THE ZERO ORDER FIELD- TONE THE FIRST ORDER FIELD.  THE ARRAY GIVES
C THE TEMPERATURE AT NTEMP POINTS FROM Y=0 TO Y=1
C
      DIMENSION T(1001)
C
C     CALCULATE ZERO ORDER FIELD
C
      PI=3.1415926
      FN1=FS**(0.5)
      CFN1=COS(FN1)
      TFN1=2.*FN1
      DY=1./(NI-1)
      DO 2  J=1,NI
        Y=DY*(J-1)
        X=(1.+Y)*PI/2.
        TZERO=(COS(FN1*Y)-CFN1)/CFN1/FS
C
C     CALCULATE FIRST ORDER FIELD
C
        SUM=0.
        FK3=4.*FS/PI/PI
        DO 3 JI=1,NS
          FNP=JI*PI/2.
          FK1=SIN(FNP)
          FC1=TFN1+FNP
          FC2=TFN1-FNP
          A=SIN(FC1)/4./FC1+SIN(FC2)/4./FC2+FK1/FNP/2.
          A=A*PI*FK1
          FC1=FN1-FNP
          FC2=FN1+FNP
          B=SIN(FC1)/2./FC1+SIN(FC2)/2./FC2
          B=-B*2.*PI*FK1*CFN1
          NC=1-(-1)**JI
          C=CFN1*CFN1*NC/JI
          FJIS=JI*JI
          ASUM=(A+B+C)*FJIS/2./(FJIS-FK3)
          ASUM=ASUM*SIN(JI*X)
    3     SUM=SUM+ASUM
        TONE=-SUM/FS/FS/CFN1/CFN1
        TONE=TONE*2./PI
    2   T(J)=TZERO+FKP*TONE
      RETURN
      END
```

```
FORTRAN IV G LEVEL  21                SIMPS              DATE = 70104          15/01/34

0001              SUBROUTINE SIMPS(H,A,N1,N2,AREA)
            C
            C   THE SIMPS SUBROUTINE USES SAMPSON'S RULE TO INTEGRATE AN ARRAY
            C
0002              REAL MIDSUM
0003              DIMENSION A(1001)
0004              ENDSUM=0.
0005              MIDSUM=0.
0006              NI=(N2-N1)/2
0007              J=N1-1
0008              DO 1 I=1,NI
0009                 J=J+1
0010                 ENDSUM=ENDSUM+A(J)
0011                 J=J+1
0012           1     MIDSUM=MIDSUM+A(J)
0013              AREA=H*(2.*ENDSUM+4.*MIDSUM-A(N1)+A(N2))/3.
0014              RETURN
0015              END
```

ORIGINAL PAGE IS
OF POOR QUALITY